Lappeenranta–Lahti University of Technology LUT

LUT School of Engineering Science

Master's Programme in Chemical and Process Engineering

Toni Laurikainen

ZETA POTENTIAL IN LIME MUD EVALUATION

Master's thesis

Examiners: Professor Antti Häkkinen

D.Sc. Teemu Kinnarinen

Instructor: M.Sc. Mikko Suhonen

TIIVISTELMÄ

Lappeenrannan-Lahden teknillinen yliopisto LUT
LUT School of Engineering Science
Master's programme in Chemical and Process Engineering

Toni Laurikainen

Meesan ominaisuuksien arviointi zetapotentiaalin mittauksella

Diplomityö

2019

78 sivua, 30 kuvaa, 6 taulukkoa, 5 liitettä

Tarkastajat: Professor Antti Häkkinen
D.Sc. Teemu Kinnarinen

Hakusanat: meesan ominaisuudet, meesan suotautuminen, kaustisointi, kalkkikierto

Diplomityön tarkoitus oli tutkia zetapotentiaalimittausten soveltuvuutta meesan laskeutumis- ja suotautumisominaisuuksien ennustamiseen, sekä ylikalkittumisen havaitsemiseen. Ylikalkittuminen liitetään usein moniin käyttöongelmiin sellutehtailla kuten meesauunin kohonneeseen polttoaineen kulutukseen, viirojen tukkiutumiseen suodatuksessa, sekä renkaiden muodostumiseen meesauunissa.

Kirjallisuusosassa käsiteltiin laskeutumisen, suodatus- ja zetapotentiaalin teoriaa. Kalsiitin zetapotentiaaliin vaikuttavat tekijät on esitetty, mukaanlukien kalkin fyysiset ja kemialliset ominaisuudet jotka vaikuttavat kalkin sammumis- ja kaustisointireaktioihin. Aiempia töitä liittyen zetapotentiaalin hyödyntämiseen ylikalkittumisen havainnointiin on tarkasteltu.

Kokeellisessa osassa tarkoituksena oli toistaa ja varmistaa aiemmissa töissä esitettyjä tuloksia. Tämän lisäksi tarkasteluun otettiin meesan pesun vaikutus zetapotentiaalin mittaustuloksiin, sekä virtauspotentiaalin soveltuvuus ylikalkittumisen havainnointiin. Kaustisointikokeet tehtiin käyttämällä synteettistä viherlipeää ja poltettuja kalkkinäytteitä, jotka toimitettiin suomalaisilta sellutehtailta. Meesanäytteille suoritettiin laskeutus-suodatuskokeet joiden jälkeen näytteiden zetapotentiaalit mitattiin.

Edellisten töiden tulokset varmistuivat. Zetapotentiaalia voidaan hyödyntää ylikalkittumisen havainnointiin. Meesan pesulla todelliin olevan mitätön vaikutus mitattuun zetapotentiaaliin. Tämän työn tulosten perusteella virtauspotentiaalimittaus ei sovellu ylikalkittumisen havainnointiin, mutta tulosten todentaminen vaatii lisätutkimusta.

ABSTRACT

Lappeenranta-Lahti University of Technology LUT
LUT School of Engineering Science
Master's programme in Chemical and Process Engineering

Toni Laurikainen

Zeta potential in lime mud evaluation

Master's thesis

2019

78 pages, 30 figures, 6 tables, 5 appendixes

Examiners: Professor Antti Häkkinen
D.Sc. Teemu Kinnarinen

Keywords: lime mud evaluation, lime mud filterability, causticizing, lime cycle

Aim of this master's thesis was to study applicability of zeta potential measurement in lime mud evaluation and overliming detection. Overliming in causticizing has been linked to a number of operational problems throughout a pulp mill, notably increased lime kiln fuel consumption, lime mud filter plugging and lime kiln ring formation.

In the literature review filtration, settling and zeta potential theory have been studied. Factors affecting calcite zeta potential have been identified, including physical and chemical properties of lime which affect causticizing and slaking reactions. Previous works paving the way for overliming detection in causticizing were also reviewed.

In the experimental part, the objective was to replicate findings from previous studies and confirm them. Additionally, the effect of lime mud washing on lime mud zeta potential and streaming potential measurements were studied. Slaking and causticizing reactions were performed using synthetic green liquor and reburned lime samples from different pulp mills in Finland. Settling and filtration tests were performed on lime mud samples, afterwards zeta and streaming potentials were measured.

Finding in previous studies were confirmed. Zeta potential could be utilized as a mean to detect overliming in causticizing. Lime mud washing had a negligible effect on measured zeta potential. Based on the results on this study, streaming potential cannot be utilized in overliming detection. However, further studies are required to confirm these results.

ACKNOWLEDGEMENTS

I would like to thank my supervisors Antti Häkkinen, Teemu Kinnarinen and Mikko Suhonen for their help, guidance and expertise throughout the project. Additionally, I want to show my gratitude towards Tiia Fíner for guidance and participation in the project and, Teija Laukala for general help and troubleshooting with the selected equipment. I also want to thank my family and friends for their given support throughout my studies.

Toni Laurikainen

Helsinki 9.11.2019

Contents

ABBREVIATIONS

CE %	Causticizing degree
EDL	Electrical double layer
IEP	Isoelectric point
LR	Liming ratio
NPE	Non-process element
PDI	Potential determining ion
PZC	Point of zero charge

SYMBOLS

A	filtration area (m^2)
C	solids concentration by volume fraction (m^3/m^3)
c	mass of dry solids in cake per volume of filtrate (kg/m^3)
c_i	concentration of ion species (mol/L)
d	particle diameter (m)
F	Faraday constant (C/mol)
g	gravity acceleration (m/s^2)
I	ionic strength (mol/L)
K	Kozeny coefficient (-)
k	permeability (m^2)
Δp	pressure difference (Pa)
P_s	solids compressive pressure (N/m^2)
Q	volumetric flow rate (m^3/s)
R_g	universal gas constant (J/K mol)
R_m	resistance of the filter medium (1/m)
S_v	specific surface area per unit volume (m^2/m^3)
t	time (s)
T_0	absolute temperature (K)
U	settling velocity (m/s)
u_t	terminal settling velocity (m/s)
V	volume of filtrate (m^3)
V_c	cake volume (m^3)
V_v	void volume (m^3)
w	weight of the filter cake (kg/m^2)
x_{sv}	Sauter mean diameter (m)

z_i	valency of an ion species (-)
α	specific cake resistance (m/kg)
α_{av}	average specific cake resistance (m/kg)
ε	porosity (-)
κ	dielectric constant (F/m)
μ	liquid viscosity (Ns/m^2)
ρ	liquid density (kg/m^3)
ρ_s	solid density (kg/m^3)
Ψ	sphericity (-)

1 Introduction

Kraft pulping was discovered in 1879 which at that time offered many benefits such as much faster delignification rate, yielding stronger pulp and lesser carbohydrate degradation due to shorter cooking times. The first Kraft mill went into operation in 1890 in Sweden and nowadays is the dominant process used in pulping. [1]

Kraft pulping is a chemical pulping method which uses sodium hydroxide (NaOH) and sodium sulfide (Na_2S) at pH above 12 and temperatures in range of 160-180 °C. The goal is to dissolve fiber binding lignin as much as possible. Kraft process can be used for any wood species yielding high strength pulp, it is tolerant to bark and has an efficient energy and chemical recovery cycles. Some disadvantages of Kraft process are need for pulp bleaching and sulfur emissions which are odorous. [1]

Overliming has been linked to several problems which can occur throughout the mill. These problems include boilover at the slaker, carryover of particulate in the white liquor and the production of low-density lime mud. Boilover is much more likely to occur when using reburned lime since it can enter the slaker at temperatures of 400 °C or higher. Presence of unreacted $Ca(OH)_2$ usually results in slow settling mud which may result in high lime mud carryover in the clarified white liquor. This can lead to scaling problems in the digester and can increase the chlorine demand in the bleach plant or even discolor the pulp grey. [2] Pulp mills using precoat filters may experience plugging which is thought to be caused by the small particle size of $Ca(OH)_2$ [3].

The presence of free lime usually produces low density lime mud. Higher moisture content present in lime mud decreases lime kiln fuel efficiency drastically. [4] In addition, a greater volume of mud has to be then removed from the white liquor clarifier increasing the pumping rate. A higher concentration of white liquor will be present in the mud washer. This in turn may lead to increased concentration of sodium compounds and lime mud carryover in weak wash due to poor settling characteristics. Latter may increase dregs concentration in the smelt dissolving tank and in the unclarified green liquor. Presence of $Ca(OH)_2$ makes the mud more difficult to wash which results in high sodium concentration and can affect the calcination of lime mud. [2]

2 Recovery process in Kraft pulping

The recovery cycle of Kraft process in principle consist of recovery of inorganic cooking chemicals, generation of heat energy by burning organic materials derived from wood, reduction in pollution and chemical usage by conversion of waste products into useful materials, and regeneration of the inorganic chemicals into pulping chemicals. The recovery process consists of liquor cycle and lime cycle. [1] Flowsheet of kraft pulping recovery cycle is shown in Figure 1.

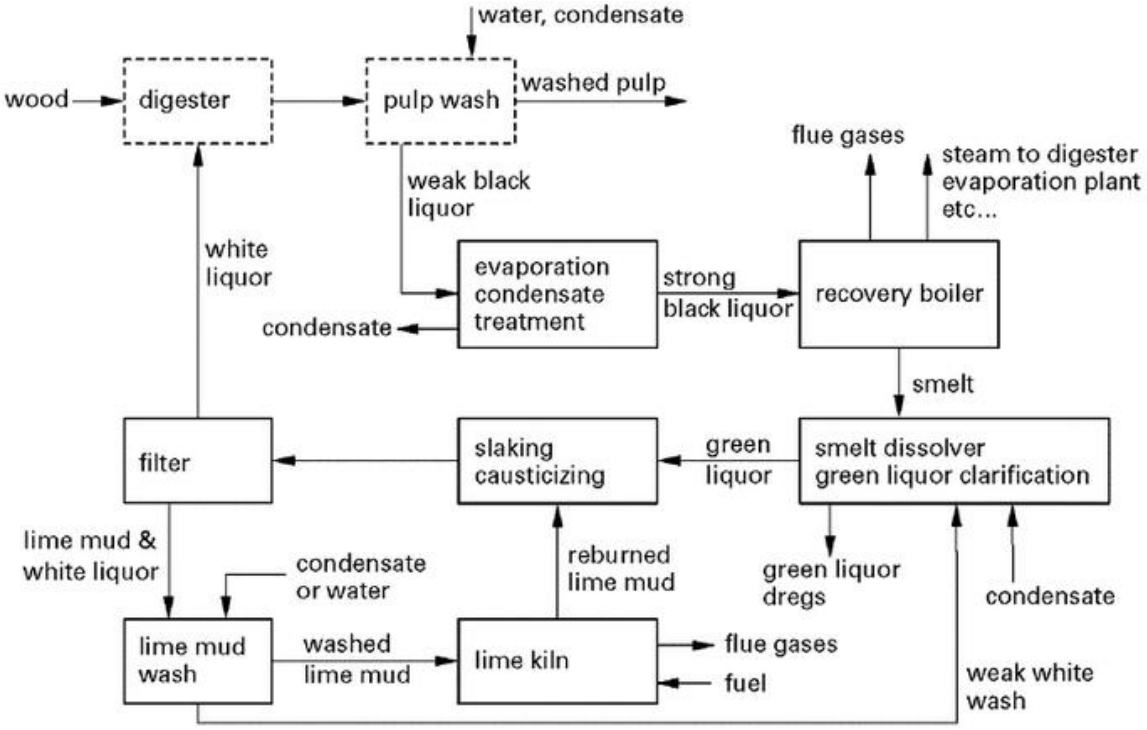

Figure 1 Flowsheet of kraft process recovery cycle [5].

Weak black liquor is first concentrated by evaporation to increase the efficiency of heat recovery from liquor combustion. Black liquor is burned in the recovery boiler at 65-73 % solids content typically. The purpose of the recovery boiler is to recover the inorganic chemicals in the form of smelt, burn organic chemicals to prevent them discharging as pollutants, and to recover the heat generated in combustion in the form of steam. Chemical reactions in the recovery boiler are conversion of sodium salts and reduction of sodium sulfate (Na_2SO_4) to Na_2S:

$$2\,NaOH + CO_2 \rightarrow Na_2CO_3 + H_2O$$

$$Na_2SO_4 + 4C \leftrightarrow Na_2S + 4\,CO$$

Inorganic pulping chemicals discharge from the bottom of recovery boiler as molten smelt which is dissolved into water yielding green liquor and it is clarified. The density of green liquor is used as a process control variable of its concentration. Green liquor clarifier is a settling tank and the main goal of clarification is to remove dregs (undissolved materials) via sedimentation. Clarifier can also be used as a mean of storage for green liquor for a short time supply. Dreg removal can be also achieved by filtration, which is a more modern approach. Dregs removal is done to prevent accumulation of inert non-process elements (NPEs) which reduce lime availability. Dregs are washed in a dregs washer, where 90-95 % of the sodium chemicals are removed. [1]

Lime (CaO) is added to green liquor (at 99-105 °C) in a slaker which results in both slaking and causticization reactions taking place simultaneously:

Slaking: $CaO(s) + H_2O \rightarrow Ca(OH)_2(s)$

Causticizing: $Na_2CO_3(aq) + Ca(OH)_2(s) \leftrightarrow 2\ NaOH\ (aq) + CaCO_3(s)$

Slaking reaction is very fast and usually reaches completion within 10 minutes. The reaction is highly exothermic, reaction heat being 1160 kJ/kg CaO. Average particle size within slaker varies with the quality of reburned lime (normally between 15-30 um). The slurry passes a classifier before it is passed on to causticizers. Classifier separates particles which have not been sufficiently disintegrated, which are referred as lime grits. Lime grits consist of reburned lime with a high degree of sintering and may also contain high concentrations of NPEs. [5]

Causticizers are continuous flow and stirred reactors (two to four in series) which are used to complete the causticizing reaction with a total retention time of 1.5 to 2.5 hours. White liquor is then clarified and, as green liquor clarifiers they can be used as a mean of short-term storage. White liquor clarifiers are settling tanks which are used to separate lime mud from the white liquor. Lime mud ($CaCO_3$) leaves the white liquor clarifier at a solids content of 35 % and higher to minimize entrained soda that is removed in the lime mud washer. Poor lime mud settling may be result of overliming (lime addition in the slaker), a low lime availability (below 80-85 %), or inadequate white liquor clarification. White liquor can be further clarified by using white liquor pressure filters. [1, 5]

Lime mud particles are agglomerates and the size can vary from couple of μm to 100 μm. Mechanical forces of mixing within slaking and causticizing vessels affect the structure of lime mud agglomerates by disintegration. Lime mud particle size reduces as slaking and causticizing reactions progresses due to these mechanical forces which may be described as grinding. Reburned lime characteristics are known to affect lime mud particle size. [5]

Entrained alkali within lime mud is removed by lime mud washing. If lime mud was not washed, the Na_2S would cause slagging in the lime kiln during calcination and reduced sulfur compounds would be released as H_2S. Washing water (weak wash or weak white liquor) is used to dissolve smelt from the recovery boiler. Approximately 1 % alkali remains within the lime mud after washing. [1] One or two washing steps are used. Rotary drum filters are typically used in one step washing. The first stage of two step washing is a simple dilution-separation operation followed normally by a use of rotary drum filter. [5]

Washed lime mud is diluted to 25-30 % solids before filtration. Lime mud filter is a rotary drum vacuum filter washer which is used for final lime washing and thickening to 60-70% solids content. Water removal is important for increasing lime kiln efficiency. After thickening lime mud enters the lime kiln where it is dried, heated and ultimately converted back to CaO by calcination reaction:

Calcination: $$CaCO_3(s) \rightarrow CaO(s) + CO_2(g)$$

Retention time in the lime kiln is between 2-3 hours. Typically, a rotary kiln is used but some mills use a fluidized bed calciner. Rotary kilns are 2.4 to 4 m in diameter and 30 to 120 m long. A lime kiln has three distinct heating zones, where at first lime mud is dried, then heated and at the end of lime kiln calcination occurs at a temperature approximately 1200 °C. [1]

2.1 Liquor and lime analyses

Lime availability

Reburned lime purity is described by lime availability which is defined as:

$$lime\ availability = \frac{CaO}{lime}\ (as\ mass\ ratio)$$

Decreased availability is caused by low temperature within lime kiln or excess moisture of entering lime mud. [1]

Total titratable alkali (TTA)

TTA is the sum of all bases within white liquor which can be titrated with strong acid. Generally included chemicals are NaOH, Na_2S and Na_2CO_3 however, small amounts of Na_2SO_3 and other acids might be present. TTA value can be reported as g/L of NaOH or g/L of Na_2O. [1]

$$TTA = NaOH + Na_2S + Na_2CO_3$$

Active alkali (AA)

AA is used to describe the amount of active ingredients in the pulping process (NaOH and Na_2S). AA values can be reported as g/L of NaOH or g/L of Na_2O. [1]

$$AA = NaOH + Na_2S$$

Effective alkali (EA)

EA includes the ingredients which will produce alkali under pulping conditions. Commercially, EA value of 12-18 % is used to produce unbleached pulp and 18-24 % to produce bleached pulp. Hardwood species require lower amount of EA due to lower lignin content present in the wood. EA value can be reported as g/L of NaOH or g/L of Na_2O. [1]

$$EA = NaOH + \frac{1}{2}Na_2S$$

Sulfidity

Sulfidity describes the ratio of Na_2S to the active alkali and is reported as percentage. Typically mills operate at 24-28 % sulfidity, but this depends largely on the wood species being pulped. Sulfidity increases delignification rate which occurs by nucleophilic action of hydrosulfide anion (HS^-). Low sulfidity leads to higher lignin content and high degree of carbohydrate degradation which leads to low strength pulp. Excess sulfidity increases emissions of reduced sulfur compounds and may increase equipment corrosion rate. All chemicals are expressed as equivalent amount of NaOH or Na_2O. [1]

$$Sulfidity = \frac{Na_2S}{NaOH + Na_2S} * 100\ \%$$

Causticizing efficiency (CE %)

Causticizing efficiency is the ratio of NaOH to NaOH and Na2CO3. CE % is used to describe the efficiency of the causticizing process. Spent NaOH in cooking is converted back to useful NaOH from Na_2CO_3 in the causticizing cycle. A target CE value of 78-80 % is typically used in commercial pulp mills. All chemicals are expressed as equivalent amount of NaOH or Na_2O. [1]

$$CE\ \% = \frac{NaOH}{NaOH + Na_2CO_3} * 100\ \%$$

3 Settling theory

Particle suspension can be separated into four classification based on their solids concentration and morphology. Type I suspension have low solids concentration and do not flocculate. The contained particles are discrete and do not interfere with one another during settling. Type II suspensions consist of particles which are able to agglomerate. As the size of agglomerates grows, they settle faster. At higher solids concentrations (than Type I and II suspensions) hindered, or Type III settling occurs. In hindered settling a blanket of particles is formed. The blanket traps particles bellow the interface resulting in a clear interface above the blanket. The settling velocity of the blanket depends on the solids concentration, as solids concentration increases the settling velocity decreases. At much higher concentrations than are found in Type III settling, compression settling or Type IV settling occurs. Particles may not really settle, instead fluid drains out of a mat of particles (a paste or cake) very slowly. Type IV suspensions are found in dewatering operations. [6]

In a dilute suspension, individual particles settle based on their size and density and do not interact with one another. A particle settling vertically in a fluid is affected by gravitational, buoyant and drag forces. The acceleration of the particle occurs due to imbalance in forces. As the particle velocity increases, buoyant force remains constant and drag force increases until force balance is reached. When constant velocity is reached (terminal settling velocity) the sum of drag and buoyant forces equal gravitational force. [6]

Terminal settling velocity in a laminar flow regime for Type I suspensions can be determined using Equation (1):

$$u_t = \frac{d^2}{18\mu}(\rho_s - \rho)g \tag{1}$$

Where, u_t terminal settling velocity (m/s)

μ liquid viscosity (Ns/m^2)

d particle diameter (m)

ρ liquid density (kg/m^3)

ρ_s solid density (kg/m^3)

g gravity acceleration (m/s^2).

Equation (1) is known as Stokes' law and applies for spherical particles in an infinite fluid. The applicability of Stokes' law has two restrictions. Particle concentration should be so low that the settling particle is not affected by the presence of any neighbors and the particle Reynolds number should be less than 0.2. When these conditions are met, the settling is called "free settling". There is no distinct interface between settling solids and the liquid that results in a cloudy suspension which clarifies over time as solids are deposited on the bottom of the settling vessel. [7]

Hindered settling (Type III) occurs when the settling velocities of particles are affected by the presence of other particles. The movement of the fluid which is displaced by the particle motion has a little impact on the drag force. However, when solids concentration is high enough, a settling particle experiences increased frictional forces due to restriction of fluid velocity fields affected by high particle concentration. [6] In this case, the settling rate is related to the terminal settling velocity of the particles and the porosity raised to a power that is a function of the particle Reynolds number:

$$U = u_t \varepsilon^n \tag{2}$$

Where, U settling velocity of the particle suspension (m/s)

ε porosity.

The exponent *n* in Equation (2) varies from 2.39 to 4.65 depending on the particle Reynolds number and on the diameter of the sedimentation vessel [7].

Development of a distinct interface is an important feature of hindered settling. The concentration of solids deposited on the bottom of the sedimentation vessel increases as time passes which causes the layers of constant concentration to appear moving upwards. At the same time the interface between clear liquid and the settling solids is moving downwards. The change of this interface with time is known as the batch settling curve. The typical features of a batch settling curve are illustrated in Figure 2. [7]

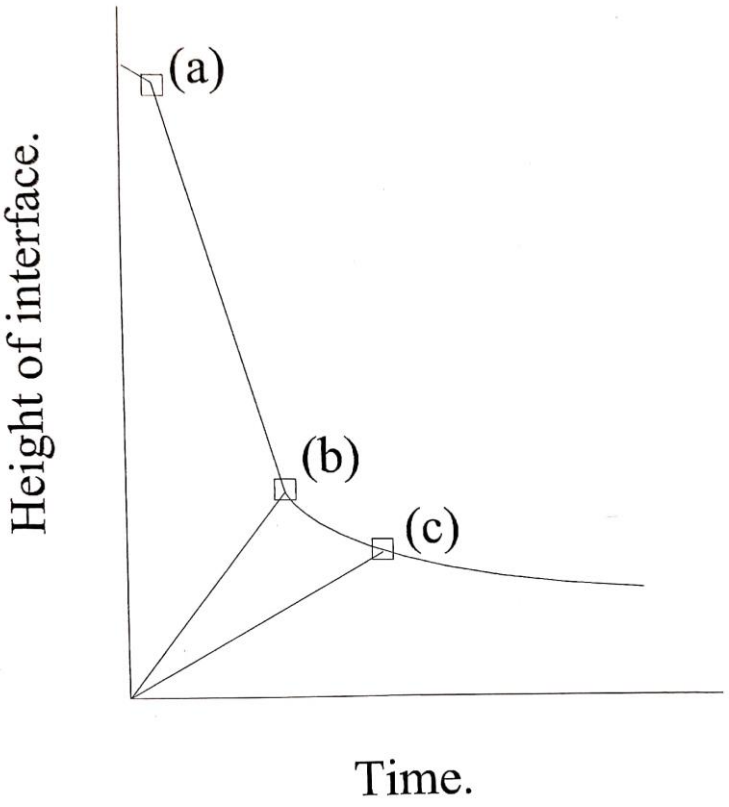

Figure 2 Illustrated batch settling curve [7].

During the introduction period, up to point (a), the suspension recovers from initial disturbances or loosely aggregated particles are formed. From point (a) to (b) a constant rate of fall of the interface is observed. At point (b) there is a transition to a first falling rate section which ends at point (c), the "compression point", beyond which is a second falling rate section. At the compression point particles are in direct contact with one another marking the end of the hindered settling regime. [7]

In the settling of concentrated suspensions a following force-momentum balance applies:

$$\frac{\partial P_s}{\partial x} = Cg(\rho_s - \rho) - \frac{\mu}{k}U \tag{3}$$

Where, P_s solids compressive pressure (N/m^2)

C solids concentration by volume fraction

k permeability (m^2)

U settling velocity (m/s).

There are three forces which affect the particle which are the buoyed weight of the solids in the layer, the liquid drag as a result of the motion of particle layer and the solids stress gradient which can transmit particle weight by point contact through a network of contacts. [7]

When the particle sedimentation does not possess a continuous contact of solids, the stress gradient becomes zero and Equation (4) can be rearranged:

$$U = Cg(\rho_s - \rho)k/\mu \tag{4}$$

If the particle size distribution is known, it is possible to estimate the batch settling velocity from Equation (4).

Permeability can be calculated from Equation (5):

$$k = \frac{\varepsilon^3}{K(1-\varepsilon)^2 S_v^2} \tag{5}$$

Where, K Kozeny coefficient

S_v specific surface area per unit volume (m^2/m^3)

ε local porosity.

The expression of permeability from Equation (5) is substituted in Equation (4). This gives Equation (6) which can be used to estimate batch flux. The Kozeny contant K usually has the value of 5 for packed beds and 3.6 for moving beds.

$$UC = \frac{g(\rho_s-\rho)(1-C)^3 x_{sv}^2 \psi^2}{36K\mu} \tag{6}$$

Where, x_{sv} Sauter mean diameter

Ψ sphericity

K Kozeny coefficient.

Differentiating Equation (7) gives an expression for the propagation velocity:

$$\frac{dh}{dt} = -\frac{g(\rho_s-\rho)3(1-C)^2 x_{sv}^2 \psi^2}{36K\mu} \quad (7)$$

Equation (7) assumes that the initial concentration is uniform and increases from the bottom of the suspension as time passes. The settling velocity approaches zero when solids concentration approaches a maximum value at the sediment layer deposited at the bottom of the vessel. [7]

4 Filtration theory

Filtration may be defined as the separation of solids from liquids by passing a suspension through a permeable medium which retains the solid particles. Fluid flow through the filter medium is obtained by applying a pressure drop across the medium. The driving forces which may be used are gravity, vacuum, pressure and centrifugal.

Two types of filtration processes are used in practice: surface filters are used for cake filtration and depth filters are used in deep bed filtration. In cake filtration the suspended solids are deposited in the form of cake on the up-stream side of filter medium. In deep bed filtration the particle deposition takes please inside the filter medium and cake deposition on the surface is undesirable. Surface filters are used with suspensions containing higher concentrations of solids. In a depth filter the particles are smaller than the filter openings which allows them to travel inside the pores until they are attached to the medium by molecular and electrostatic forces.

The whole pressure drop is available at the beginning of a batch cake filtration. As the cake starts to build up, pressure drop decreases resulting from an effective increase in cake resistance leading to a gradual drop in the flow rate. Thus the cumulative filtrate volume slows down as filtration progresses. [8]

The flow rate Q through a filter cake and a filter medium can be calculated using Equation (8) which is based on Darcy's equation:

$$Q = \frac{\Delta pA}{\alpha \mu w + \mu R_m} \tag{8}$$

Where, Q volumetric flow rate (m^3/s)

Δp pressure difference (Pa)

A filtration area (m^2)

α specific cake resistance (m/kg)

w weight of the filter cake (kg/m^2)

R_m resistance of the filter medium (1/m).

However, if the volume of filtrate at each moment of time is known, it is more convenient to use the integrated Equation (9).

$$\frac{t}{V} = \frac{\alpha_{av}\mu c}{2A^2\Delta p}V + \frac{\mu R_m}{A\Delta p} \tag{9}$$

Where, t time (s)

V volume of filtrate (m^3)

α_{av} average specific cake resistance (m/kg)

c mass of dry solids in cake per volume of filtrate (kg/m^3).

The specific cake resistance should be constant for incompressible cakes. However, most cakes are compressible and their specific resistance changes with pressure drop. Therefore, an average specific cake resistance is used. [8] The average specific cake resistance for incompressible cakes can be related to the Sauter mean diameter of particles and the average porosity of filter cake by a modified Kozeny-Carman equation:

$$\alpha_{av} = \frac{180(1-\varepsilon_{av})}{\rho_s {x_{sv}}^2 {\varepsilon_{av}}^3} \tag{10}$$

The average porosity of the whole filter cake can be calculated from Equation (11).

$$\varepsilon_{av} = \frac{V_v}{V_c} \tag{11}$$

Where, V_v void volume (m^3)

V_c cake volume (m^3).

The volume of the cake can be calculated on the basis of its height and cross-sectional area. The void volume of the cake can be determined by subtracting volume of suspended solids from the cake volume. [9]

Equation (9) is a straight line, where t/V is the dependent and V is the independent variable. Plotting the gathered data points of t/V against V allows calculation of the slope and intercept of Equation (9):

$$Slope = \frac{\mu c \alpha}{2A^2 \Delta p}$$

$$Intercept = \frac{\mu R_m}{A \Delta p}$$

If liquid viscosity, filter area, filtration pressure and mass of dry cake per unit volume of filtrate are known, the graphically determined values of slope and intercept can be used to calculate cake specific resistance and filter medium resistance. [7]

5 Physical properties of lime and lime quality

Reburned lime consist of agglomerates of CaO crystallites with large openings between the crystallites. Diameter of the largest crystallites is typically in range of 6 to 8 μm. The formation of these larger crystallites is probably due to sintering of 2 to 4 μm crystallites. [10]

5.1 Sintering

Sintering is a generic term which refers to phenomenon where particles are fused together. This results in loss of specific surface area as when two particles are fused the bridge between the particles (neck) grows. As particles are fused together, the particle size grows. [11] Although reburned lime could have a high degree of porosity, the reactivity towards water is extremely low. While high porosity is often accompanied by high surface area, in case of lime pellets the specific surface areas are often very low. This is due that there is no porosity between calcium oxide crystallites other than large voids between non-porous solid bodies. Lime pellets may be either soft and easily pulverized, or hard and difficult to crush. [12] Soft reburned lime is more reactive in the causticizing process but leads to small lime mud particles. Hard reburned lime on the other hand leads to large lime mud particles which are more preferable in white liquor separation. [11] Typically the size of lime pellets is in range from 5 to 50 mm. In extreme cases, lumps or balls may be formed in the lime kiln with a diameter larger than 100 mm. Pellets smaller than 20 to 30 mm in diameter have typically low residual carbonate content and larger pellets consist of a dark un-calcinated grey core which is surrounded by a white calcinated shell. [13]

The decrease of specific surface are for lime is influenced by temperature, residence time and the composition of surrounding atmosphere and impurities found in lime mud. The atmosphere within the lime kiln contains CO_2 which is formed during the thermal decomposition of lime mud, but is also supplied by hot flue gasses. CO_2 has been identified to enhance sintering of lime. Recarbonation is likely to occur if CO_2 levels reach close to or above of equilibrium for calcination/recarbonation reaction, which will decrease specific surface area of lime greatly. [11] Commandré [14] observed that the composition of the atmosphere and the calcination temperature affected both the specific surface area and the hydration activity of quicklime. Two types of sintering were observed for lime samples; thermal and chemical sintering. Higher CO_2 concentration in the atmosphere was observed to increase the time to extinguish for quicklime samples with the same specific surface area.

5.2 Lime quality

Limes used in the pulp mill are classified as active or unreactive. The available lime content is essentially the same as the reactive lime content for active limes. For unreactive limes, the available lime content can be significantly higher than reacting lime content. Active limes have a small crystallite size (about one micron) and are porous. Unreactive limes have a much larger particle size and so have a smaller surface area, and are considerably less porous. Slaking reaction occurs rapidly and all the CaO is converted into $Ca(OH)_2$ when active lime is used. The smaller surface area of the unreactive lime hinders the slaking reaction and compared to active lime, the reaction occurs more slowly. [2]

Campbell [2] compared the chemical and physical properties of purchased quick lime and reburned lime. Settling rate decreased rapidly when purchased lime was used at causticizing efficiency above 80 %. This was like due to the presence of unreacted $Ca(OH)_2$ which is known to affect lime mud settling rate. A similar trend was also observed with reburned lime. However, due to lower porosity and so lower reactivity compared to purchased lime the settling rates were observed to be slower than that when using purchased lime. Above 80 % causticizing efficiency when using purchased lime the volume of lime mud increased and lime mud density decreased due to effect of unreacted $Ca(OH)_2$ on the lime mud settling properties. A similar trend was also observed when using reburned lime, however the mud volume was found to be considerably higher at equivalent causticities and so the mud density was lower. Usage of fresh lime in a pulp mill can lead to operational problems if the increased reactivity of the fresh lime is not taken into account. Although the available lime content between reburned and fresh limes are similar, the reacting lime content in reburned lime is much lower. Purchased lime will usually contain at least 10 % more reactive lime which could overlime the system. [2]

5.3 Effect of lime physical properties on slaking and causticizing

The surface area of lime particles influences the slaking time; lime with high surface area reaches reaction completion faster than lime with low surface area. Dorris [12] found this relationship to be linear when testing the slaking properties of lime samples acquired from 10 different mills. Limes with higher slaking rates also exhibit a higher rate of causticizing and the decrease in the rate after rapid rise in causticizing efficiency occurs shortly after the completion of slaking reaction. The rate-determining step of the causticizing reaction is

suggested to be the internal diffusion of the carbonate ions towards the unreacted core and the diffusion of hydroxide ions towards the exterior of the solid phase.

Dorris [10] observed that the surface area of reburned lime increased from 0.4 to 50 m^2/g upon hydration. This is due a large number of $Ca(OH)_2$ crystallites being formed on the surface of the CaO pellet. As slaking reaction progresses, the CaO pellets start to disintegrate due to rapid expansion of outside layers of the pellet. The 1.98-fold increase in molar volume causes swelling of the outside layers which in turn causes cracking and splitting of the outside layers. However, a drop in surface area of the fully hydrated lime particles was observed. As the hydration progresses towards the center of the CaO pellets, progressively smaller in size $Ca(OH)_2$ particles are liberated which are able to re-agglomerate or re-crystallize forming less porous structures.

Reaction rate of causticizing is influenced by the surface area of the calcium species within the solution. Initial hydration of CaO forms high surface area $Ca(OH)_2$ crystallites which promotes fast initial causticizing rates. Carbonation of $Ca(OH)_2$ leads to a loss of the newly formed surface which causes the causticizing reaction to slow down. Formed $CaCO_3$ particles are both larger in size and less porous when compared to $Ca(OH)_2$ particles. [10] Precipitated $CaCO_3$ is able to form a coating around unreacted CaO particles. This results in inhibition of the slaking reaction and some CaO will not be available for the reaction due to encapsulation of CaO particles by $CaCO_3$. [2] The size of lime mud particles was found to be related to the size of CaO primary crystallites in the pellets. Thus, more reactive lime produces lime muds smaller in particle size which transmits into slower settling times. [12]

6 Zeta potential theory

Zeta potential describes the magnitude of the electrostatic repulsive forces between charged particles in a liquid. Commonly zeta potential is used to predict and control dispersion stability. [15] For smaller particles (< 10 μm) electrostatic forces may become as significant as gravitationally or hydrodynamically induced forces [16].

Electrical double layer (EDL) is formed around a charged particle to neutralize the surface charge which causes electrokinetic potential between the particle surface and suspending liquid. The voltage difference can be measured and is referred to as the surface potential. Surface charge and thickness of the EDL are related to the magnitude of this surface potential. [17]

The net repulsive forces between particles tend to increase with increased solids load. Reduction of the magnitude of repulsive forces causes dispersion to become unstable promoting coagulation. The repulsive forces between particles can be reduced either increasing ionic concentration by adding a non-adsorbing electrolyte, or by altering the particle surface charge by a specific adsorption of certain ions or charged polymers. Generally, when zeta potential is close to zero faster settling rates and improved filterability can be expected. At the maximum or minimum zeta potential slower settling rates and decreased filterability are expected due to greater repulsion forces between the particles which prevents particle agglomeration. [16] Generally, if the absolute value of zeta potential is 30 mV, dispersion is considered electrostatically stable [18].

6.1 Electrostatic stability of colloidal dispersions

Colloidal electrostatic stability is observed in dispersions with low solids loads and is usually explained by the Derjaguin-Landau-Verwey-Overbeek (DLVO) theory for the interactions between charged particle pairs [19]. In general, particles are affected by a very weak attraction force at large distances (secondary energy minimum), an electrostatic repulsion at intermediate distances and a strong attraction at short distances (primary energy minimum) [20]. The total potential interaction energy between particle pairs results from the balance between repulsive potential due to overlapping of particles electrical double layers (EDLs), and the attractive potential due to long range van der Waals dispersion forces [15]. Van der Waals attraction results from forces between individual molecules in each colloid. The effect of dispersion forces is additive as each molecule of the first colloid has a van der Waals

attraction to each molecule in the second colloid. DLVO model is visualized in Figure 3. [17]

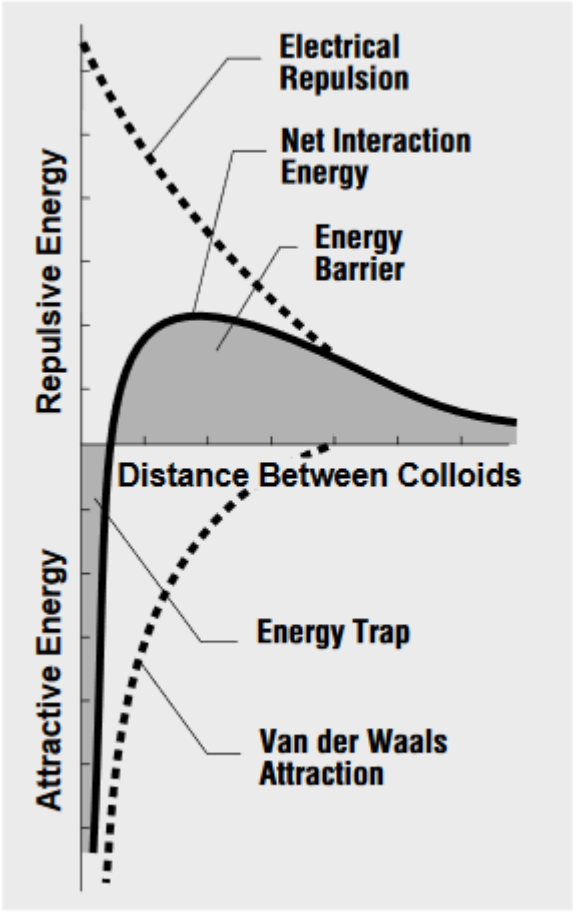

Figure 3 Forces taken into account in DLVO theory visualized [17].

Suspensions are stable and unable to coagulate when the repulsive potential is high. This is due the total potential remains positive even for long distances. [19] The point of maximum repulsive energy is called the energy barrier and the height is related to system stability. At this point in order for colloids to coagulate the particles must have a sufficient kinetic energy in collisions to jump over the energy barrier. [17] If the repulsion potential decreases, attractive secondary minimum can be observed and particles are able to cluster at this distance. However, strong short-range repulsive forces keep the particles from direct contact. Increasing ionic concentration reduces the thickness of EDL and the repulsive potential can be reduced so that particles fall into a deep attractive primary minimum and are able to coagulate. [19]

6.2 Development of electrical double layer

Development of electrical charges at particle surfaces results from adsorption/desorption of ionic species in solution which are dictated by dissociation equilibria. Electrical double layer (EDL) surrounds charged particles due to attraction of counter-ions to the particle surface. [19] Additional counter-ions repel each other by the ones in the Stern layer which are still attracted to the particle surface. The dynamic equilibrium which result from this is called diffuse layer, which is shown in Figure 4. The concentration of diffuse layer decreases as the distance from the particle surface increases and gradually reaches equilibrium concentration of bulk solution. Co-ions which have a same charge as the particle are initially repelled by the surface charge of the particle. The concentration of co-ions increase with distance from the particle surface as the repulsive forces of particle surface decrease until equilibrium is reached. [17]

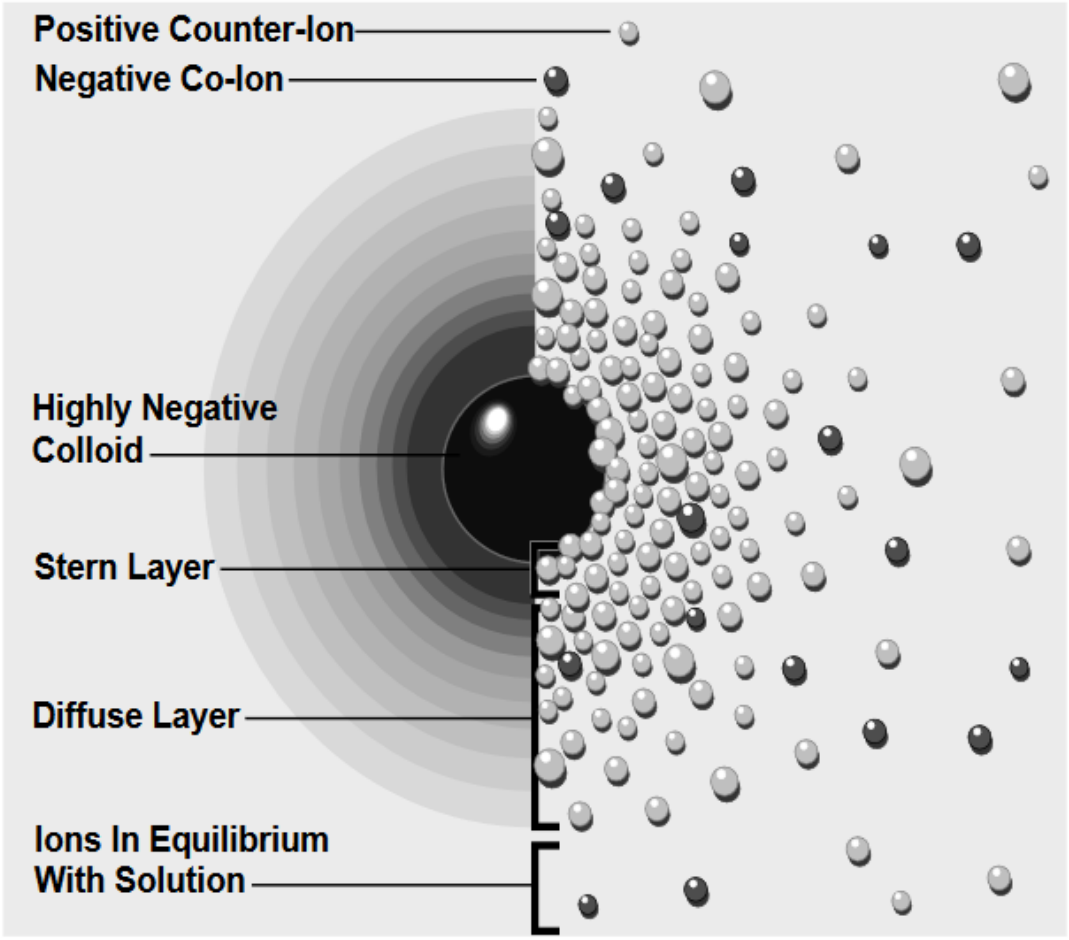

Figure 4 Development of electrical double layer [17].

Stern layer exists immediately adjacent to the particle surface and contains ions which are attached to the particle surface. The Stern layer can be further divided into the inner and outer Helmoltz layers (IHP and OHP). Ions which closely approach the particle surface and are attached to the surface sites are located on the IHP. Larger hydrated ions that cannot enter the IHP but are attached to the particle surface are located on the OHP. The difference between Stern and diffuse layers is that the co- and counter-ions in the diffuse layer are not attached to the particle surface. The electrical potential within EDL decreases linearly from the particle surface through the Stern layer and exponentially from the OHP through the diffuse layer. [21]

The thickness of EDL can be characterized with Debye length l_D that estimates how far the electrostatic effect of surface charges range. Increased ionic strength I causes EDL to shrink closer to the particle surface. Debye length is independent of the surface properties of particle and is only affected by liquid parameters. [22] The shrinking of diffuse double layer decreases zeta potential in magnitude [21].

$$I = \frac{1}{2}\sum_i z_i^2 c_i \tag{11}$$

Where, z_i valency of a ion species (-)

c_i concentration of ion species (mol/L).

$$l_D = \sqrt{\frac{\epsilon R_g T_0}{2IF^2}} \tag{12}$$

Where, κ dielectric constant (F/m)

T_0 absolute temperature (K)

R_g universal gas constant (J/K mol)

F Faraday constant

I ionic strength (mol/L).

6.3 Electrokinetic phenomena

Electrokionetic phenomena arise when charged particles are set in a relative motion in respect to the polar liquid phase. The movement of charged particles or the liquid near the charged surface causes the appearance of electric potential. The most known electrokinetic phenomena are electro-osmosis, streaming potential, electrophoresis and sedimentation potential. All electrokinetic phenomena are related to the development of electrical double layer around the particle. [23]

The electrophoretic mobility relates to the dielectric constant and viscosity of the suspending liquid and to the electrical potential at the slip plane. Slip plane is defined as the point where the Stern layer meets diffuse layer. While the Stern layer is rigidly attached to the particle surface, diffuse layer is not. The electric potential at the slip plane is related to electrophoretic mobility and is called the zeta potential. [17] As mentioned above, there are four general methods to measure zeta potential:

1) Electrophoresis: the movement of a charged particle in an external electric field is relative to the stationary fluid.
2) Electro-osmosis: the movement of the liquid in an external electric field is relative to the stationary charged particles which are placed e.g. in a porous plug.
3) Streaming potential, the opposite to electro-osmosis: electrical potential gradient is generated when liquid is forced through a porous charged plug by pressure.
4) Sedimentation potential, the opposite of electrophoresis: electrical potential gradient is generated when charged particles settle or float (depending on particle density) relative to a stationary fluid. [24]

6.4 Effect of pH on zeta potential of metal oxides

Charge development for most metal oxides occur when mineral surface sites are hydrated to form amphoteric groups which can react either with H^+ or OH^- ions. The number of negatively and positively charged surface sites depend on the H^+ and OH^- concentration in the solution, which behave as potential determining ions (PDIs). The net surface charge/zeta potential depends on the solution pH. As pH increases zeta potential becomes increasingly negative as deprotonation reaction is favored and more positive as pH decreases which favors the protonation reaction. [21]

Deprotonation: $MeOH^0 + OH^- \leftrightharpoons MeO^- + H_2O$

Protonation: $MeOH^0 + H^+ \leftrightharpoons MeOH_2^+$

The point of zero charge (PZC) occurs when the number of positively and negatively charged sites is equal. Zeta potential and electrophoretic mobility of zero may also be observed and the corresponding pH is referred as the isoelectric-point (IEP). [21, 24]

6.5 Zeta potential of calcite

The surface of calcite differs from other metal oxides in several ways. Calcite is soluble in aqueous solution and the lattice ions Ca^{2+} and CO_3^{2-} can be released into solution or deposit on the surface depending upon pH of the solution. Atmospheric CO_2 can dissolve into solution affecting pH and the equilibrium concentrations of Ca^{2+}, CO_3^{2-} and HCO^{3-} ions. [21, 25]. Calcite surface contains also protonated anion surface sites and hydroxylated cation sites which are dependent on pH. However, several studies have shown that the zeta potential of calcite is independent of pH if Ca concentration is kept constant. [21] Increase in solution alkalinity decreases zeta-potential because CO_3^{2-} ions start to dominate Ca^{2+} ions. Presence of Na_2CO_3 in calcite suspension has been found to makes zeta potential increasingly negative. [24] Zeta potential measurements of calcite rely on using electrokinetic phenomena. Other techniques which are used to determine surface charge such as potentiometric titration are challenging to apply in calcite. This is due rapid dissolution kinetics and buffering effect of carbonate ions in solutions which may affect the results. [21, 26]

A strong dependence between zeta potential and excess of Ca^{2+} ions at the mineral surface has been observed [21]. Increasing calcium concentrations has been found to shift zeta potential to more positive values due to Ca^{2+} adsorption onto negative surface sites [24]. The charge development of calcite surface is more complex compared to simple protonation and deprotonation reactions which occur at the surface sites of metal oxides. This is due to ability of the adsorbed lattice ions Ca^{2+} and CO_3^{2-} to go through complexation reactions. [21]

Studies on the zeta potential of calcite have produced somewhat contradictory results. In some studies only negative or positive zeta potential values have been obtained and the IEP values reported range from pH 5.4 to 11. Researchers have suggested that this behavior may be due on the nature of the calcite sample, differences in solid/liquid ratios of the suspension,

vigorous shaking and the presence of atmospheric CO_2. [24] Natural calcite contains trace amount of organic matters which alters the surface charge compared to synthetic calcite [27].

Several studies have concluded that the potential determining ions (PDIs) for calcite are Ca^{2+} and CO_3^{2-}. Other studies have suggested that H^+, OH^-, $CaOH^+$ and HCO_3^- ions can act as PDIs. Other ions are also able to adsorb directly to the calcite surface which is dependent on the physicochemical properties such as charge, size, molecular structure and water solubility. Generally polyvalent ions (PO_4^{3-}, HPO_4^{2-}, SO_4^{2-}, CO_3^{2-}, Mg^{2+}, Ca^{2+}) are able to change the surface charge due to adsorption onto opposite-charged surface sites and/or precipitation of another mineral onto the calcite surface. [24] Mg^{2+} has been found to behave identically to Ca^{2+}, increase in Mg^{2+} concentration shifts zeta potential to more positive values. SO_4^{2-} has been observed to affect the zeta potential of calcite by decreasing it as its concentration increases. However, it is not clearly concluded yet that SO_4^{2-} is a PDI. [21]

6.6 Zeta Potential as a possible monitoring technique

Azgomi [28] studied the impact of liming ratio on lime mud settling and filterability. In the study, Azgomi used pure CaO and reburned limes obtained from pulp mills. Since liming ratio did not considerably change lime mud particle size, which was hypothesized, the effect of surface charge on the settling and filterability was studied. Zeta potential measurements of lime mud particles as function of LR showed that zeta potential increased as LR increased. This phenomenon was consistent for all lime types used in the study. The zeta potential was slightly negative when the system was underlimed and became strongly positive when the system was overlimed.

Increasing free lime resulted in higher zeta potential which suggested that difficulties in settling and filterability may be caused by increase in repulsive forces between the particles. The relationship between zeta potential and the increase in free lime content appeared to be linear. Azgomi implied that measuring zeta potential could be used to predict filterability of the lime slurry.

A correlation between the zeta potential of lime mud particles and causticizing efficiency (CE) was found. Increasing CO_3^{2-} concentrations caused zeta potential to shift towards more negative values which correlates to low CE. The maximum CE could be attained at the zero value for zeta potential when Ca^{2+} and CO_3^{2-} concentrations are equal in the suspension.

Overliming causes zeta potential to shift increasingly more positive values. Thus, the magnitude of the zeta potential depends on the Ca^{2+} and CO_3^{2-} concentrations.

7 Mill closure and accumulation of non-process elements

Stricter environment regulations and advancements in process integration techniques have been the main factors driving efforts toward improvements in water management and wastewater reduction in pulp and paper industry. Accumulation of non-process elements (NPEs) have risen a major concern in development of closed cycle operations. [29] NPEs are classified as elements which are not essential to the chemical processes in the mill and have a detrimental effect to pulping, bleaching or recovery [30, 31, 32]. NPEs enter the process cycle with wood, makeup chemicals, process water, from the bleach and with any waste streams which are disposed within the process [33]. The control of NPEs is important since different elements have a tendency to accumulate in different cycles leading to operational problems and dead load [30]. NPEs can be classified into three general groups:

1) Elements which are highly soluble in alkali and are able to build up without a limit (K and Cl).
2) Elements which are partially soluble in alkali and build up to significant levels before precipitation (Al, Si, P).
3) Elements which are highly insoluble in alkali and are purged by green liquor dregs therefore not building up (Ca, Mg, Ba, Fe). [33]

While Na and Ca are used in mill chemical processes, technically Na becomes an NPE when it is admitted into the lime cycle and Ca when it is admitted into the sodium cycle. Operational problems caused by accumulation of NPEs may cause deposits and corrosion of equipment in the liquor recovery cycle and in the bleaching plant equipment such as washer screens, filtrate tanks, nozzles, repulpers, piping and instrumentation. In addition to these problems, NPEs are responsible for increased lime kiln fuel use, reduced lime mud settling and filtration efficiency. [29, 34] Incineration of secondary sludge in the recovery boiler has been of interest to the pulp industry due to favorable economics. There are some concerns regarding this practice since it increases the load on process equipment, and is also a potential source of NPEs. Sludges may contain significant levels of aluminum which is troublesome by causing scaling and reduces lime mud filterability. [33, 35]

7.1 NPE sources and properties

Non-process elements enter the cycle with wood, chemical makeup, process waters, fuels used in lime kiln and secondary sludge, if it is burned in recovery boiler. In the following section the sources and chemical properties of notable NPEs are discussed.

Sodium (Na)

Sodium compounds in lime mud are either water-soluble, water-insoluble or guarded sodium. Water-soluble Na is derived from the white liquor residual in the lime mud consisting mainly from cooking chemicals but small amounts of Na_2CO_3, Na_2SO_4 and NaCl are also present. Water-insoluble Na is chemically bound in silicates which reduces solubility in water. It is formed in reactions between water-soluble Na and silica or silicate minerals in the lime mud or refractory bricks of the lime kiln. Guarded Na is insoluble in water at room temperature, but becomes soluble when it is exposed in high temperatures. The formation mechanism of guarded sodium is not fully understood. Guarded Na cannot be controlled in the lime mud by washing. Na has the highest concentration of the NPEs found in the lime cycle. The low melting point of sodium compounds enhance sintering and may contribute to ring formation in the lime kiln. [36] Sodium compounds found in the dissolving tank deposits are pirssonite (Na_2CO_3•$CaCO_3$•$2H_2O$) and thermonatrite (Na_2CO_3•H_2O). These sodium compounds may be carried over from clarifier dregs into lime mud. [34]

Calcium (Ca)

The main sources of calcium are wood and make-up lime. If good clarification and filtration occurs, Ca is confined in the lime cycle. The main problem of Ca in the recovery cycle is the scaling in the evaporation plant. Higher evaporation temperatures invokes deactivation of Ca, reduces solubility of Ca and reduces scaling. [31]

Silica (Si)

Silica enters the pulping process through wood, make-up chemicals, process water and biofuels when it is used in the lime kiln. Scandinavian wood contains 0.01-0.05 wt-% Si. The use of annual plants as feedstock greatly increases input of Si and increases the accumulation in the lime cycle. The major outputs for Si are the pulp, green liquor sludge

and lime grits. Si in green liquor reacts with CaO forming calcium silicate ($CaSiO_3$) which is linked to problems in lime mud dewatering leading to higher fuel consumption in lime kiln. Si also affects lime reburning by the formation of calcium silicates, and each 1 wt-% of Si reduces lime availability by 6 wt-%. Studies have shown that $CaCO_3$ available for decomposition was reduced from 98 % to 69 % when Si content was increased from 0 to 5.5 %. [36]

Phosphorus (P)

Phosphorus enters the system in wood, biosludge and lime kiln fuel [31, 36]. Phosphorus has a tendency to accumulate in the lime cycle due to higher solubility in green liquor than in white liquor. P levels are controlled by keeping the lime cycle partially open by not reusing all of the reburned lime. P is present in lime mud as calcium hydroxyapatite ($Ca_5OH(PO_4)_3$). In the lime kiln, most of the hydroxyapatite will form tricalcium phosphate ($Ca_3(PO_4)_2$). Lime which contains 1 wt-% of P will therefore contain 5 wt-% tricalcium phosphate which is a major deadload and reduces lime reactivity. [36]

Aluminum (Al)

Aluminum enters the process as a mineral present in wood and accumulates in the lime cycle which results in dead load and reduces dry solids content of lime mud. The formation of aluminum silicates causes glass like scaling in the evaporation plant and is difficult to remove. Lime grits and lime kiln dust particles are important Al sources. [36] Aluminum can be removed with green liquor by co-precipitation with Mg which forms a compound called hydrotalcite ($Mg_6Al_2CO_3(OH)_{16}•4H_2O$) [31, 33, 37]. However, hydrotalcite is not expected to be present in lime mud since it decomposes in the lime kiln at 900 °C [34]. The aluminosilicate compounds in black liquor evaporators have been identified as kaolinite ($Al_2O_3•2SiO_2•(OH)_4$) and gehlinite ($2CaO•Al_2O_3•SiO_2$). In the lime cycle, aluminosilicate compounds such as kaolinite and hydroxysodalite ($Na_8(AlSiO_4)_6(OH)_2•2H_2O$) are known to occur in the lime cycle. These compounds are known to have a very high surface area which may lead to low solids content in lime mud. Presence of aluminosilicates is known to color the lime mud green due to interaction of sulfides with aluminosilicates. [34]

Magnesium (Mg)

Magnesium sources include mainly wood, make-up lime and magnesium sulfate ($MgSO_4$) in oxygen delignification stage. The solubility of Mg is quite low in the liquor cycle and tends to separate with green liquor dregs, grits and lime mud. [31] The chemical properties of magnesium are similar to Ca. The magnesium carbonate ($MgCO_3$) in the lime mud goes through thermal decomposition in the lime kiln forming magnesium oxide (MgO). In the slaker, MgO forms magnesium hydroxide ($Mg(OH)_2$) which does not react during causticizing. It remains in the lime mud as $Mg(OH)_2$ and due to small particle size it then lowers the filterability of the lime mud thus reducing dry solids content of the lime kiln feed. A correlation between Mg and Al content in reburned lime exist. Together they form magnesium aluminum compounds, and therefore Mg is an important factor in Al accumulation in the lime. [36]

Iron (Fe) and Manganese (Mn)

The inputs of iron include wood, make-up lime, process water and corrosion of process equipment. Iron is insoluble in alkaline conditions and can be removed by dregs and grits as sulfide, hydroxide and/or carbonate form [31, 32]. Iron may promote ring formation in the lime kiln and increase chemical consumption in the bleach plant. [31]

Manganese enters the process with wood and process waters. It has a detrimental effect on the hydrogen peroxide (H_2O_2) bleaching stage by catalyzing the decomposition of H_2O_2. Mn can be removed with acid washing and chelation but does not cause any significant problems other than coloring the lime. [31] Dregs and grits are also purge points for Mn in the forms of $Mn(OH)_2$ and $MnCO_3$. [32]

Potassium (K) and Chlorine (Cl)

The main source of potassium is wood and, K is soluble throughout the pulping process. Potassium is enriched in the precipitator ash which may be used as a purge point. [31] Potassium content varies by wood type, for softwoods the K content is 0.8 to 1.5 wt-% while for hardwoods it is 2 to 5 wt-% (dry basis). Roots and leaves contain 2 to 10 times more K than the stem. [32] The chemical properties and concentration of K in the recovery cycle is expected to be similar to Na. It may invoke ring formation in lime kiln, but will not normally cause any other problems in the lime cycle. [36]

Chlorine enters the process with wood, make-up chemicals, bleaching chemicals, process water, biosludge and spent acid. Due to total solubility of Cl throughout the pulping process, significant outlets are different effluent streams. [31]

Potassium and chlorine lower the melting points of the ash formed in the recovery boiler thus have a significant effect on the recovery operation. High levels of K increase fouling in the recovery boiler, increases plugging tendency and causes superheater corrosion particularly in high Cl level. [29, 35] Chlorine alone has a major impact on the recovery boiler fouling and plugging and causes equipment corrosion [31, 33].

7.2 Control of NPEs

Processes that remove NPEs are referred to as kidneys. Some water soluble NPEs can be purged via effluent streams and non-soluble NPEs filtration and screening processes serve as natural process kidneys. [29] The recausticizing plant is a major purge point for many NPEs. Increased level of closure in recausticizing plant leads to build-up of Mg, Fe, Al, P and Mn until insoluble salts are formed. The accumulation of inert dissolved material decreases causticizing efficiency by increasing the ionic concentration in the solution being causticized. [32]

The aluminum level in the recovery cycle is greatly dependent on green liquor clarification and filtration, since it is the only purge point. Green liquor clarification and filtration performance can be checked by observing the lime color, since NPEs have a tendency to color both lime mud and burnt lime. [31] The NPE compounds from the green liquor are able to carry over as suspended solids or dissolved in clarified green liquor and contribute to downstream deposits and scaling [34].

Iron, manganese, calcium and magnesium are present as particulates in clarified green liquor, hence increasing clarifier efficiency will reduce their concentration. Aluminum and silicon compounds are present in clarified green liquor in dissolved form only. Thus, increasing clarifier efficiency does not reduce their concentration in clarified green liquor. [34]

Highly soluble K and Cl can be only purged with electrostatic precipitator (ESP) ash and via effluents. Dissolving ESP ash is an efficient way to remove K and Cl but leads to considerable sodium and sulfur losses. [31] Heavy metals such as arsenic, cadmium, mercury

and lead together with zinc evaporate in the recovery boiler and are condensed and enriched in ESP ash [37].

8 Experimental techniques

In the experimental part of this study the objective was to study the effect of overliming on lime mud filtration and settling properties, and evaluate lime mud zeta and streaming potential measurement as a mean to detect overliming. In this section experimental procedures and used analyzing techniques are presented.

8.1 Slaking and causticizing reactions

Causticizing and slaking reactions were performed in a 1 liter jacketed glass reactor equipped with a stirrer. The used equipment is shown in Figure 5 Temperature was controlled with a water bath at 88 °C and monitored using a digital thermometer. A volume of 400 mL of synthetic green liquor was heated up to the reaction temperature prior to lime addition. After the reaction temperature was reached, the lime was quickly poured to the reactor. The slurry contained in the reactor was continuously agitated with a motorized stirrer for 90 minutes. Liming ratio (the molar ratio of CaO to Na_2CO_3) was varied to reach causticizing efficiency of 70, 80 and 85 %. Lime quantity was calculated based on how much lime would be required to achieve adequate concentration of NaOH at targeted CE % (causticizing efficiency) levels.

Figure 5 Used equipment in causticizing experiments.

Three of the limes used in this study were reburned lime samples collected from three different kraft pulp mills and one lime sample was purchased make-up lime. Lime samples were stored in airtight plastic containers with only small portion of each used for the experiments. Synthetic green liquor with a TTA (total titratable alkali) value of 180 g/L NaOH was prepared by the courtesy of Stora Enso Pulp Competence Centre. It should be noted that due to high concentration of alkali present in the synthetic green liquor, 85 % causticizing efficiency was not reached. To reach overliming conditions a generous amount of lime was added.

A volume of 300 mL of the causticizer slurry was placed in a Nutsche filter after the 5-minute settling test. The filtrate was stored in an airtight cup until the NaOH, Na_2CO_3 and Na_2S contents in the white liquor were analyzed by titration for calculation of causticizing efficiency (CE). The height and the weight of the wet filter cake of unwashed lime mud were recorded. The unwashed lime mud was then washed with tap water by making a slurry that

had a solids content of approximately 10 wt-%. The washed lime mud slurry was then filtered, and the filtrate was discarded. The height and weight of the resulted washed lime mud filter cakes were recorded.

8.2 Settling

After the slaking and causticizing reactions, the generated amount of causticizer slurry was quickly poured into a 500 mL graduated cylinder (5.82 cm ID) for a 5-minute settling. In this test the slurry is allowed to settle and a change in the height of the interface between supernatant (the clear liquid portion) and the sediment in the cylinder is measured after 5 minutes.

8.3 Filtration

After the 5-minute settling test, 300 mL of causticizer slurry was poured into a Nutsche filtration apparatus. The apparatus consisted of a 5.2 cm diameter filter cloth holder with a 350 mL chamber. The base of the filter holder was a perforated plate with a filter cloth placed on top. Pressure drop was applied to the chamber by nitrogen gas. The filtration was carried out at a constant pressure of 50 kPa. Filtration pressure in constant pressure filtration was monitored using pressure sensor. The weight of the filtrate collected in a beaker and measured with a scale. The height of the formed filter cake was measured then weighed and dried in an oven at 105 °C for 24 hours to determine moisture content. The average specific resistance α_{av} and the medium resistance R_m were calculated by plotting t/V against V and fitting a line through the data. The pressure filtration apparatus is shown in Figure 6.

Figure 6 Nutsche filtration apparatus.

8.4 Titration

CO_3^{2-}, OH^- and HS^- concentrations in the white liquor were determined by potentiometric titration using a 1.0 N hydrochloric acid (HCl) solution in accordance of SCAN-N 30:85 standard [38] for white and green liquors. The titration was conducted with an automatic titrator Mettler-Toledo T50 using Mettler-Toledo DG111-SC (3 mol/L KCl) electrode.

The liquor sample is titrated with hydrochloric acid of known concentration. From the titration curve three inflection points can be determined from which the amount of the effective, active and total alkali within the sample can be calculated. The titration analyses were performed under fume hood due to hydrogen sulfide (H_2S) being formed during titration. From the inflection points causticizing efficiency (CE %) of the liquor sample was determined according to Equations (13), (14), and (15):

$$EA = a \times \frac{\mathrm{m}}{\mathrm{V}} \quad (13)$$

Where, a is the volume of titrant to reach the first infection point (mL)

m concentration of hydrochloric acid (mol/L)

V sample volume (mL).

$$AA = (2a - 2b + c) \times \frac{\mathrm{m}}{\mathrm{V}} \quad (14)$$

Where, b is the volume of titrant to reach the second inflection point

c is the volume of titrant to reach the third inflection point.

$$TA = c \times \frac{\mathrm{m}}{\mathrm{V}} \quad (15)$$

8.5 Particle size distribution (PSD)

The particle size distribution for the lime mud samples was measured by using Malvern's Mastersizer 3000 laser particle size analyzer. Laser is used for light scattering diffraction analysis to measure particle size distribution. Smaller particles diffract light in high angles while bigger particles diffract light in lower angles. Lime mud samples were prepared in distilled water and to carry out measurements appropriate concentration were used by monitoring obscuration (5-20 %). Particle size distributions were obtained using Fraunhofer calculation model.

8.6 Zeta and streaming potential

Zeta potential (ξ) measurements were performed by using Malvern's Zetasizer Nano ZS which employs a combination of electrophoresis and Laser Doppler Velocimetry (LDV) to measure the velocity of a particle when electrical field is applied. The sample suspensions were made by adding 0.15 g of lime mud to 500 mL of distilled water at a room temperature. The pH of the suspension was adjusted to 11.5 ± 0.2 by using white liquor which was produced by the causticizing reactions.

Measurement principle is shown in Figure 7. The sample cell is equipped with electrodes which generate the required electric field for measuring zeta potential. The laser beam passes through the sample cell and is then scattered by the moving particles. The light scattered from particles is combined with the reference beam which produces an intensity signal. The

rate of fluctuation of the intensity is proportional to the speed of the particles. Once particle velocity is known, together with the strength of the applied electric field, sample viscosity and dielectric constant zeta potential can be worked out. A detector sends this information to a digital signal processor and passes it on to a computer where the included software produces frequency spectrum from which the electrophoretic mobility and zeta potential is calculated.

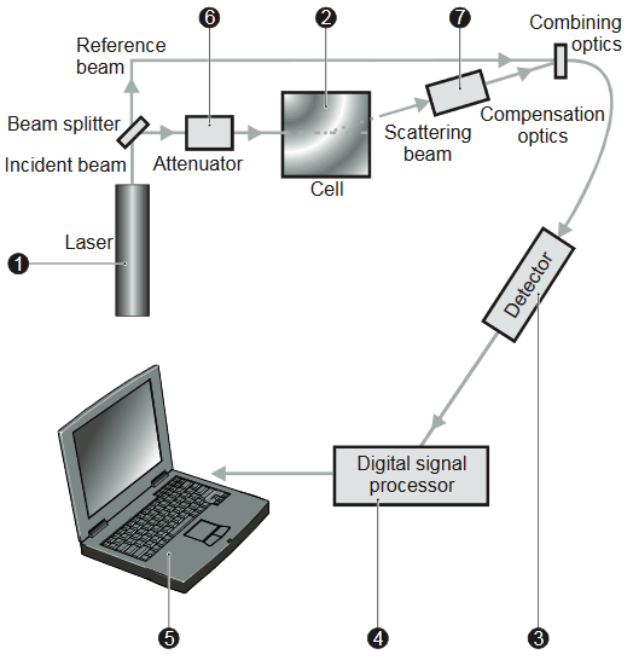

Figure 7 Measurement principle of used equipment determining lime mud zeta potential [39].

Additionally, streaming potential was measured from lime mud samples using AFG FPA touch! fiber potential analyzer. The equipment draws sample suspension via vacuum to the upper end of the measuring cell through a sieve. Suspended solids form a plug in front of the sieve which is allowed to solidify during stabilization time. Oscillating sample flow through the plug is induced with an alternating vacuum (0.2 bar and -0.4 bar) which causes the suspending liquid to drag counterion located on particle surface thus generating streaming potential which is detected by electrodes. Samples were prepared in distilled water, and sample concentration and conductivity were varied. A 30 second stabilization time was used.

8.7 Thermal gravimetric analysis (TGA)

The free lime $Ca(OH)_2$ content within the lime mud samples was measured using thermogravimetric analysis with Netzsch STA 449C QMS403C. The free lime contents of lime mud samples were analyzed for both unwashed and washed samples.

Approximately 10 mg of lime mud was weighted and placed in an aluminum sample cup. The change in sample weight was recorded as a function of temperature and samples were heated from 25 °C to 900 °C at a scanning rate of 10 °C/min in nitrogen atmosphere. The nitrogen gas was passed through the instrument at a rate of 40 mL/min. Additionally the scale had a protective helium atmosphere which flowed at a rate of 40 mL/min. The $Ca(OH)_2$ content was calculated based on the weight loss between 300 and 500 °C where $Ca(OH)_2$ decomposes to CaO.

8.8 Scanning electron microscopy (SEM)

Lime mud samples were imaged by Hitachi SU3500 Scanning Electron Microscope (SEM) to study the morphology of $CaCO_3$ particles. BSE-3D detector and 10 kV acceleration voltage were used in the imaging. A small amount of oven dried lime mud sample was used by spreading it on two-sided carbon tape.

Additionally, Energy-dispersive X-ray Spectroscopy (EDS) was used to characterize the chemical composition of the lime mud samples by using a Thermo Scientific UltraDry SSD EDS device. The EDS mapping was processed with Pathfinder software.

8.9 X-ray diffraction analysis (XRD)

The crystalline structures of lime mud samples were examined using X-ray Diffraction (XRD) Analysis. Samples were analyzed by using Brüker D8 ADVANCE diffractometer. A copper kα x-ray source at a wavelength of 1.5418 Å accompanied with kβ filter. 2θ scanning method was used in the range 10-70° with 0.02° increments each step taking 0.5 seconds.

8.10 Inductively coupled plasma (ICP-MS)

Agilent 7900 ICP-MS inductively Coupled Plasma with Mass Spectroscopy detector (ICP-MS) was used analyze the metal, phosphorus and silica contents within limes used in causticizing experiments. Lime samples were dissolved in aqua regia (molar ratio $HCl:HNO_3$ of 1:3) by weighing 0.1 g of lime and adding 4 mL of acid. The test tube was

filled to the 10 mL mark with distilled water and the solution was further diluted 50-fold in a 50 mL test tube with distilled water before analysis. A mixture of helium and argon was used as the carrier gas.

9 Experimental results and discussion

In this section results from settling and filtration tests are presented, and applicability of zeta and streaming potential measurement on overliming detection is discussed.

9.1 Characteristics of reburned lime

The reburned lime samples used in this study were identified as Lime 1, Lime 2, Lime 3 and Lime 4. The elemental composition of lime samples was determined with inductively coupled plasma paired with mass spectroscopic detector (ICP-MS). The most prominent non-process elements are summarized in Table 1.

Table 1 Non-process element contents in all lime samples analyzed by ICP-MS.

Element	**Lime 1 mg/g**	**Lime 2B mg/g**	**Lime 3 mg/g**	**Lime 4 mg/g**
Mg	14.80	8.83	10.07	7.57
Al	0.73	0.40	3.73	0.45
Mn	1.31	0.82	0.15	0.46
P	13.73	16.21	0.46	5.48
Si	2.26	1.00	4.28	1.31
Fe	0.82	0.22	2.07	0.61

Reburned lime particle size was evaluated based on particle size of lime mud formed during causticizing. Lime particle size and surface area is known to carry over to lime mud particles, as lime with small particle size tends to form lime mud small in particle size.

9.2 Lime mud settling

Lime mud settling properties were evaluated using 5-minute settling test performed in a half liter graduated cylinder. After causticizing the whole reactor contents were quickly poured to the graduated cylinder and the difference in solid/liquid interface height was measured after 5 minutes. Liming ratio was varied in causticization based on target causticizing efficiency (CE %) of white liquor. These target CE % were 70 % representing underlimed conditions, 80 % representing normal operating conditions and 85 % representing overlimed conditions. It should be noted here that due to high alkalinity of green liquor (180 g/L NaOH TTA), 85 % causticizing efficiency was not reached.

Liming ratio had a significant impact on lime mud settling rate as shown in Figure 8. This phenomenon was apparent for lime muds produced from all limes used in this study. For

example, the average settling velocity for lime mud produced from Lime 1 decreased from 1.6 cm/min at CE of 70 % to 0.4 cm/min at CE of 85 %. The effect of liming ratio of lime mud settling velocity is well known and has been extensively studied.

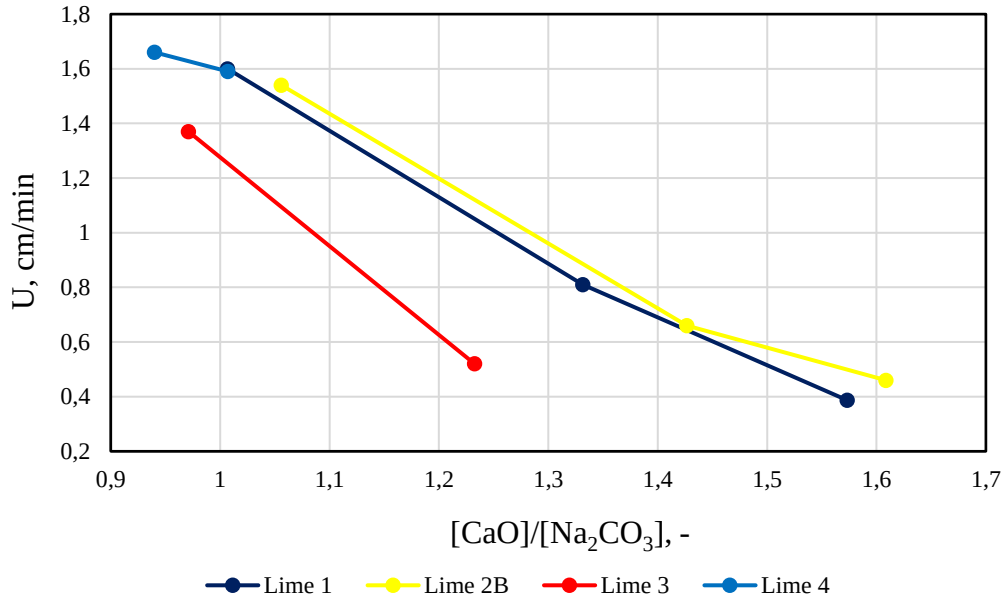

Figure 8 Average settling velocities of used limes as function of liming ratio (180 g/L NaOH TTA, 90 min reaction time)

The cause for decreased settling rate is due to formation of $Ca(OH)_2$, also known as free lime. Previously decreased settling rate was explained by smaller particle size of $Ca(OH)_2$ as in generally smaller particles tend to settle more slowly. This theory was disputed in Azgomi's [28] study, as no apparent correlation between 85th percentile diameter of lime mud particles and lime mud settling velocity was found. In Figure 9 lime mud average settling velocity is plotted as a function of average particle size (Sauter diameter). Although points in Figure 9 are layered, no concrete dependency between these two parameters was found in this study. The layering of points is caused by an apparent difference in zeta potential value. The higher a point is located in Figure 9, the lower zeta potential value was measured in the respective causticizing series.

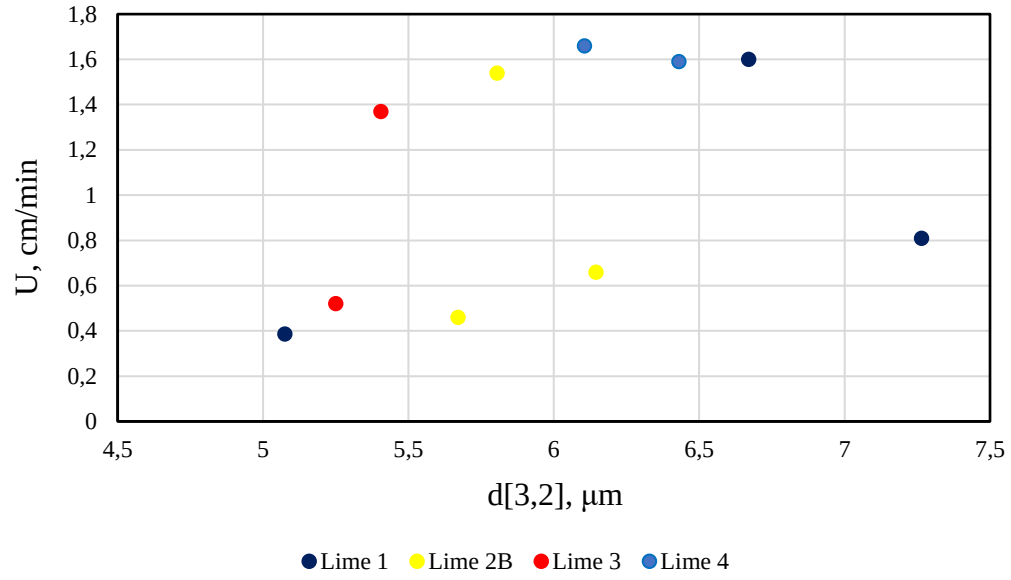

Figure 9 Comparison of lime mud particle size (Sauter mean diameter) and lime mud average settling velocity.

In Azgomi's [28] study decrease in settling velocity was identified to be caused by increase of zeta potential. The effect was also prominent in this study as presented in Figure 10. As lime mud zeta potential becomes more positive, the repulsive forces between particles increase which causes settling velocity to decrease.

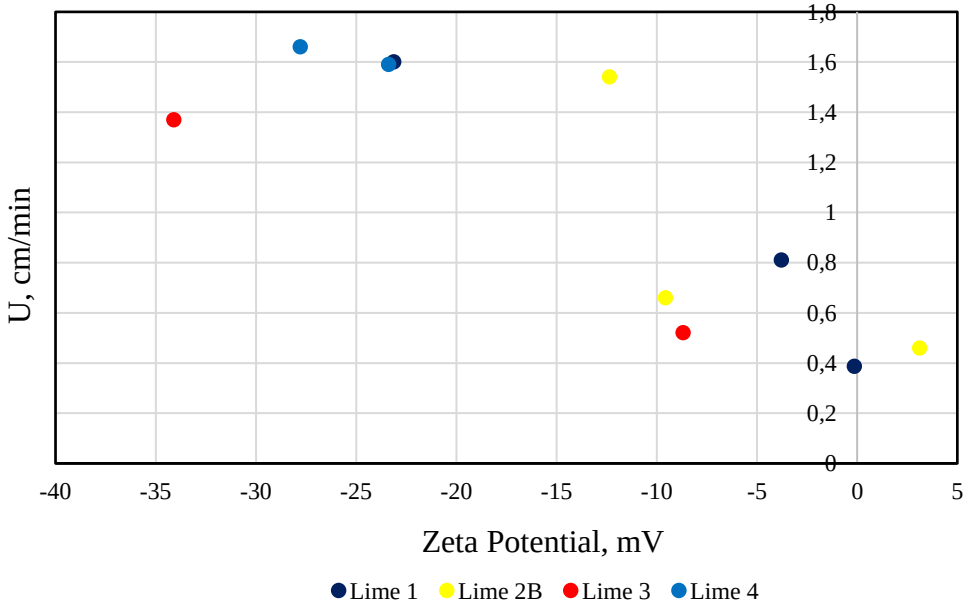

Figure 10 Average settling velocity plotted against zeta potential of lime mud particles.

9.3 Filterability of lime mud

9.3.1 Effect of liming ratio

The effect of liming ratio on lime mud filterability was studied as described in previous section. Filtration plot for unwashed lime mud produced from Lime 2B is presented in Figure 11. At higher liming ratio the time required for completion of filtration increased. The effect of liming ratio on filtration time was apparent for all limes used in this study. This is discussed in Section 9.3.2.

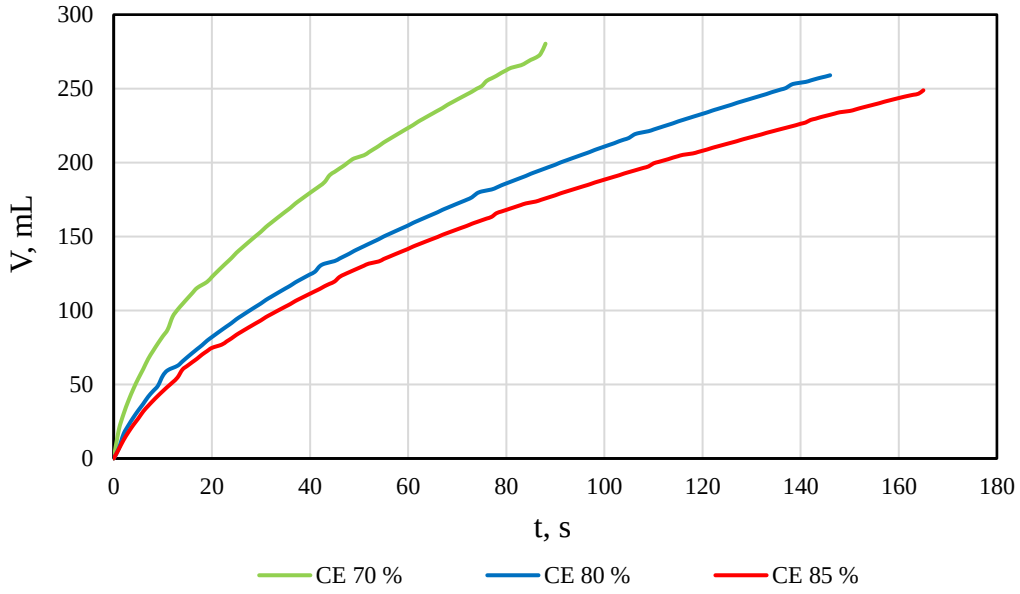

Figure 11 Filtration plot for unwashed lime mud produced from Lime 2B at specific target CE % (TTA 180 g/L NaOH, 90 min reaction time)

Filterability for the unwashed lime muds produced from Lime 2B is presented in Figure 12. In this study filterability is represented as *t/V*, time required to filter a *V* volume of filtrate. The filtration for lime mud produced at a CE 70 % finished more quickly compared to ones produced at target CE of 80 % and 85 %. This phenomenon was apparent for all lime types used in this study and is discussed in Section 9.3.2. Similar results were obtained in Azgomi's [28] work and it can be concluded that increasing liming ratio decreases the filterability.

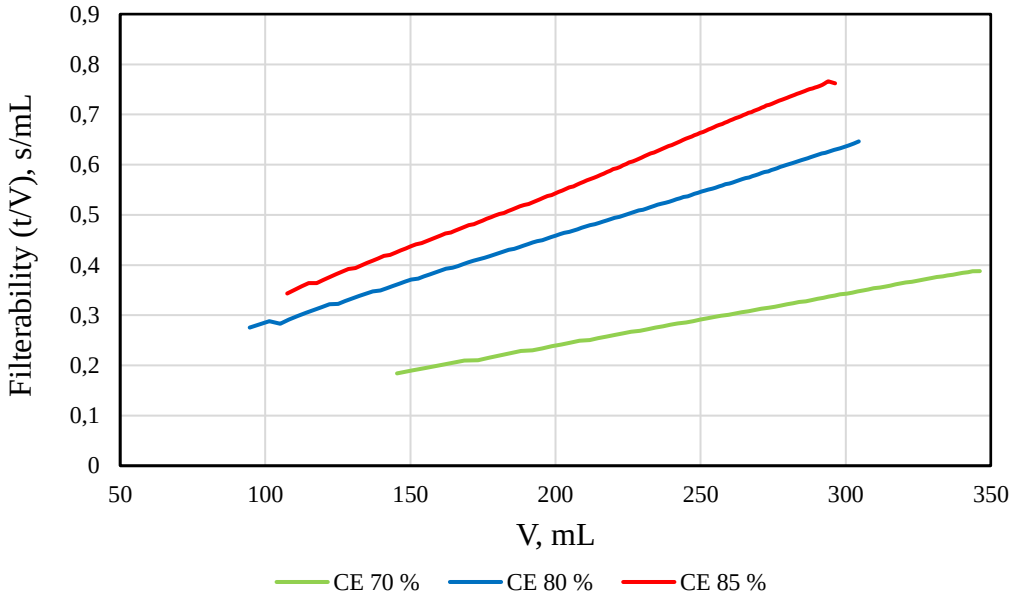

Figure 12 Filterability plot for unwashed lime mud produced from Lime 2B at specific target CE % (TTA 180 g/L NaOH, 90 min reaction time)

After the filtration experiments for unwashed lime mud were done, the effect of washing on filtration properties was studied. This was done by creating a slurry with approximately 10 wt-% solids concentration from unwashed lime mud by mixing it with hot tap water. The washed lime mud was then filtered as before and the data was analyzed. Filtration plot for lime mud produced from Lime 2B is shown in Figure 13. The time required to reach completion in filtration was significantly shorter compared to unwashed lime mud samples. Although free lime is washed off due it being more soluble in water than in alkali the filtration for lime mud produced at target CE of 85 % takes considerably longer. This can also be seen in filterability plot in Figure 14. This effect was also apparent for other limes used in this study.

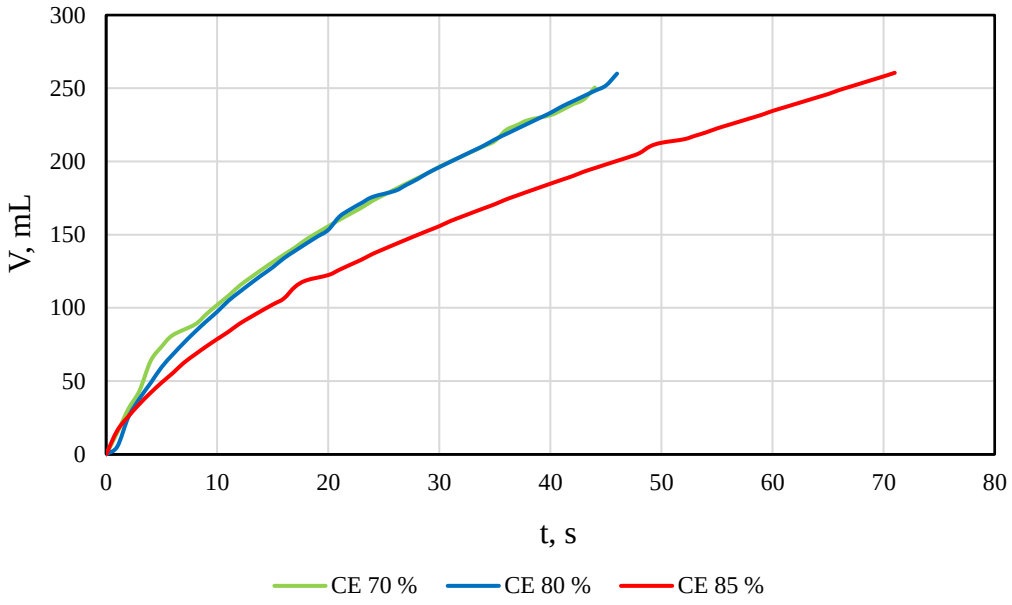

Figure 13 Filtration plot for washed lime mud produced from Lime 2B at specific target CE % (TTA 180 g/L NaOH, 90 min reaction time)

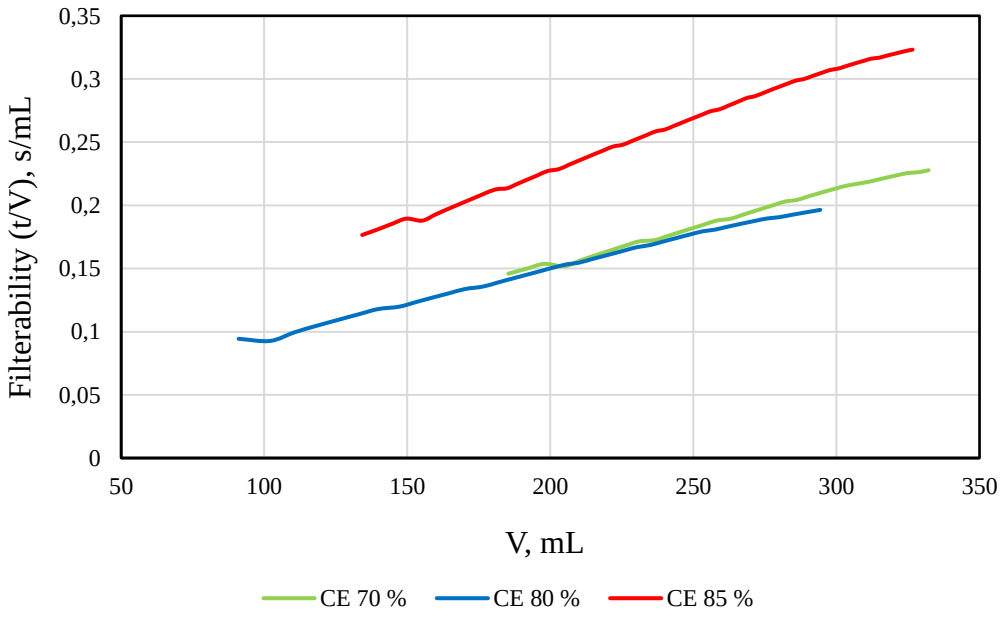

Figure 14 Filterability plot for washed lime mud produced from Lime 2B at specific target CE % (TTA 180 g/L NaOH, 90 min reaction time.

The decrease in filtration performance is mainly due to increase in liming ratio. Particle size distribution data for Lime 2B is shown in Figure 15 across used target CE %. There are no significant differences between the particle size distributions across used target CE %. The effect of particle size to filtration and settling properties for all used limes is discussed in Section 9.3.2.

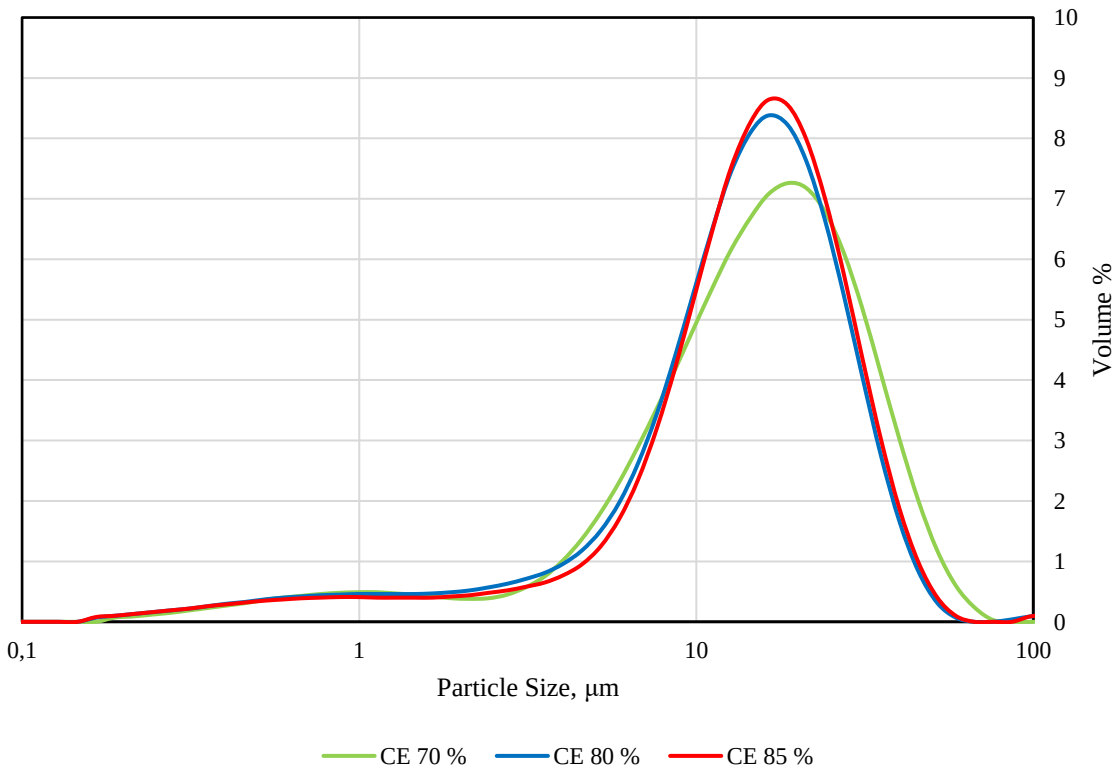

Figure 15 Volume based particle size distribution plot for lime mud samples produced using reburned Lime 2B.

Calculation of cake specific cake resistance by using Equation (9) presented in Section 4 is based on the assumption that the filter cake is incompressible. For compressible cakes the calculated cake specific resistance is pressure dependent and would be needed to be corrected according to the compressibility coefficient. The average specific cake resistance values for both washed and unwashed lime muds for all lime types are presented in Table 2.

Table 2 Calculated average specific cake resistance values for both unwashed and washed lime muds. Results for all lime types at specific target CE % are shown.

Lime Type	CE, %	Unwashed $\alpha_{av} \times 10^{10}$ (m kg^{-1})	Washed $\alpha_{av} \times 10^{10}$ (m kg^{-1})
Lime 1	70	0.429	0.336
	80	0.398	0.342
	85	0.841	0.740
Lime 2B	70	0.520	0.641
	80	0.799	0.642
	85	0.735	0.848
Lime 3	70	1.701	2.197
	80	1.853	3.003
Lime 4	70	0.338	0.346
	80	0.370	0.491

The specific cake resistance describes how formed filter cake resist the flow of the filtrate; in other words, it is a measure of filterability. A greater specific cake resistance correlates to slower filtration rate. The specific cake resistance increases as liming ratio increases, which was also concluded in Azgomi's [28] work.

However, this effect can also be seen in washed lime muds as well. The effect of liming ratio on average specific cake resistance for both unwashed and washed lime muds produced from Lime 2B is graphically presented in Figure 16 and for all lime types in Figure 17.

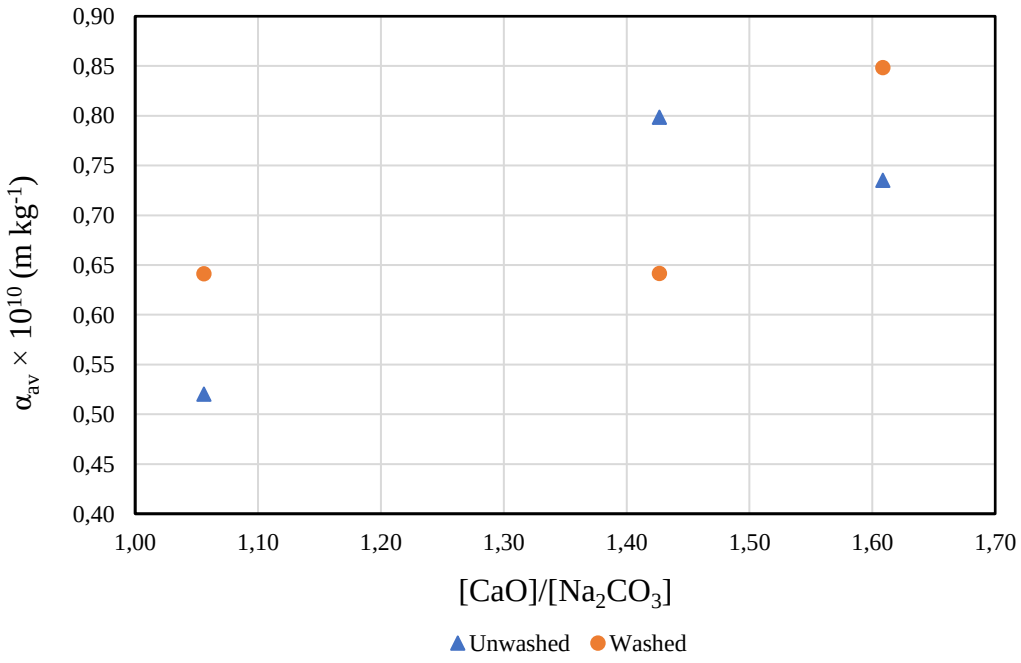

Figure 16 Average specific cake resistance plotted against liming ratio for both unwashed and washed lime mud samples produced from reburned Lime 2B.

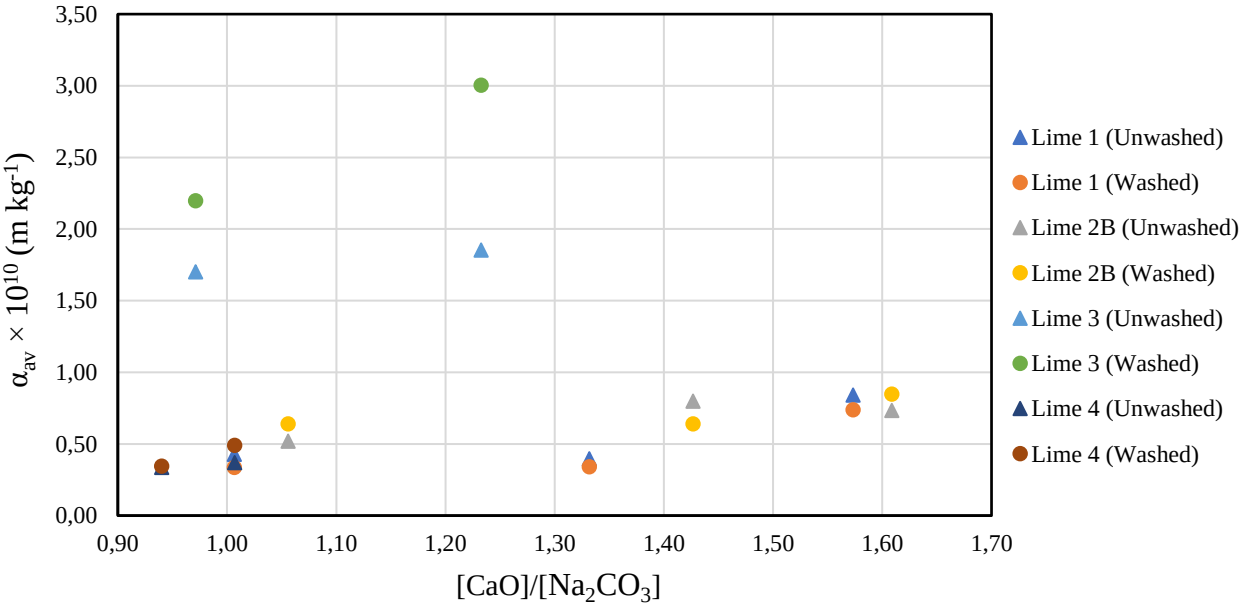

Figure 17 Average specific cake resistance plotted against liming ratio for both unwashed and washed lime muds.

Porosity describes how tightly the filter cake is packed. Particle size distribution is known to affect cake porosity; a wider particle size distribution results in more tightly packed cake since smaller particles are able to fill in voids within the cake structure. In Figure 18 average cake porosity of lime mud produced from Lime 2B is plotted against zeta potential.

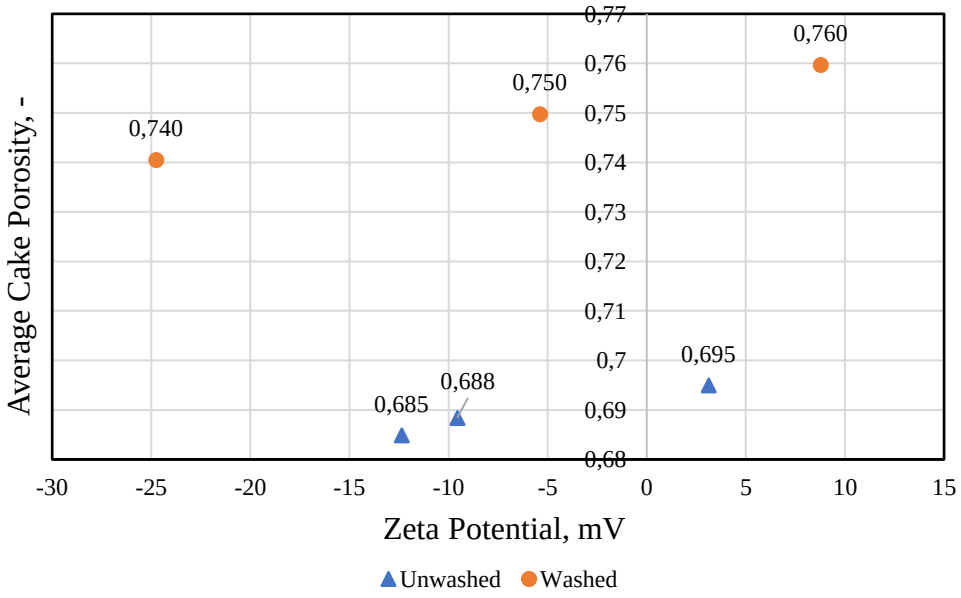

Figure 18 Average cake porosity (void volume fraction) of lime mud produced using reburned Lime 2B plotted against zeta potential for both unwashed and washed samples.

The average cake porosity seems to increase in a linear fashion as zeta potential increases and the trend is apparent for both washed and unwashed lime muds. This means that an increase in repulsive forces between the particles results in less densely packed filter cakes.

Average moisture content in lime mud filter cakes produced from Lime 2B plotted against zeta potential is shown in Figure 19.

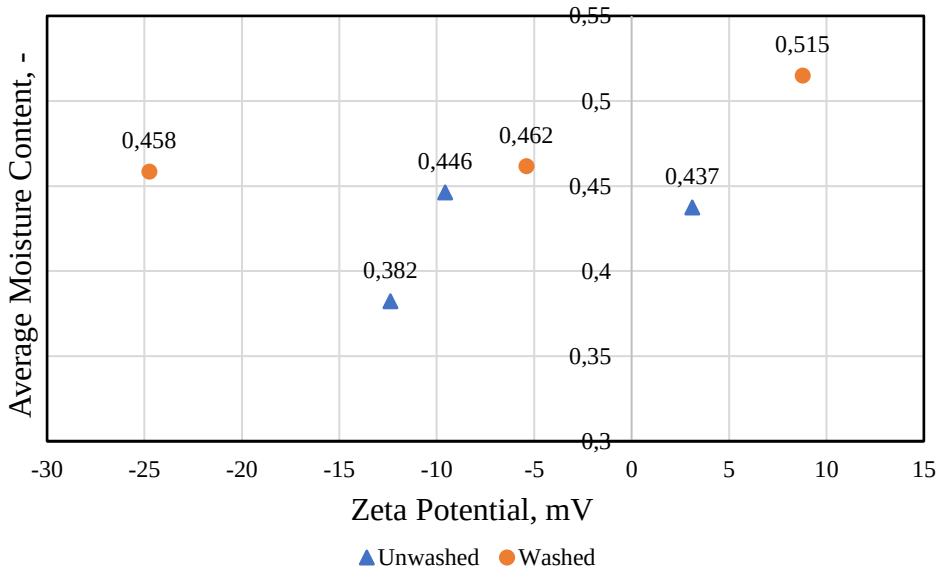

Figure 19 Average moisture content (moisture fraction) of lime mud produced using reburned Lime 2B plotted against zeta potential for both unwashed and washed samples.

The average moisture content in filter cake seems to increase as zeta potential increases. This is due to increase in repulsive forces between the lime mud particles which increases the average specific cake resistance leading to slower filtration.

9.3.2 Effect of lime type

In this section, the effect of lime type on filtration performance is discussed. The filtration plots for unwashed lime muds produced from all reburned lime samples (target CE 80 %) used in this study are shown in Figure 20 and filterability plots are shown in Figure 21.

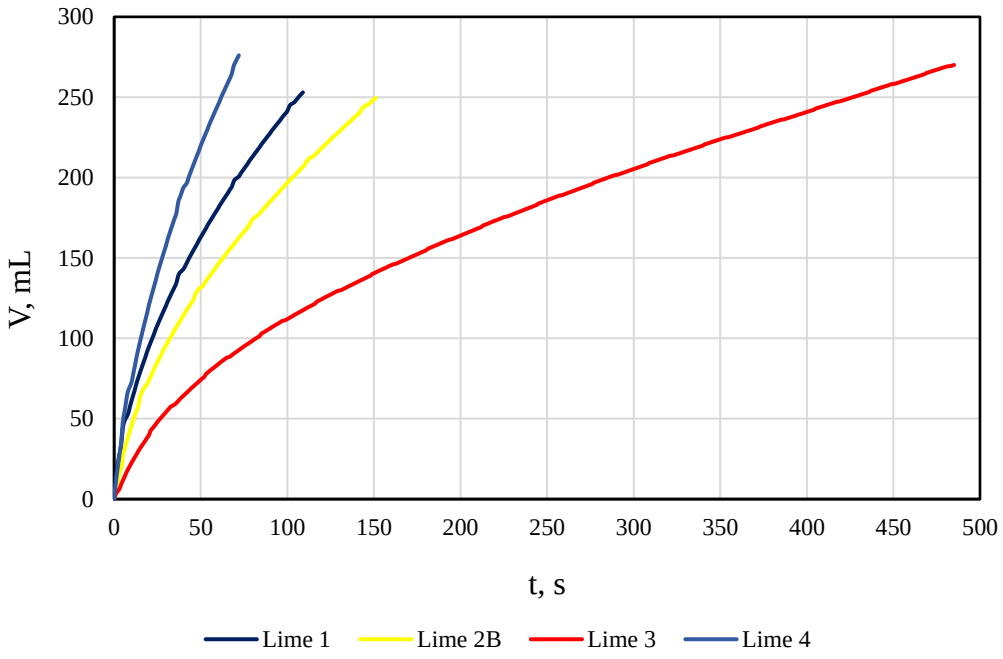

Figure 20 Unwashed lime mud filtration plot for all lime types. Target CE 80 % (TTA 180 g/L NaOH, 90 min reaction time)

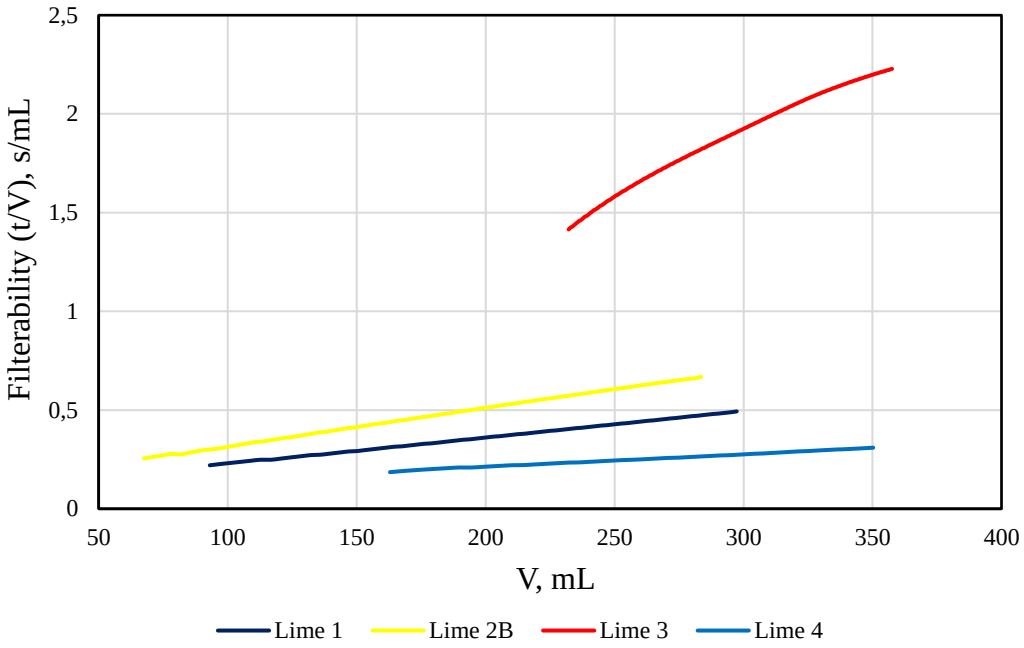

Figure 21 Unwashed lime mud filterability plot for all lime types. Target CE 80 % (TTA 180 g/L NaOH, 90 min reaction time)

Unwashed lime muds produced from Limes 1, 2B and 4 performed similarly. The filtration performance of lime mud produced from Lime 3 differs substantially. The filtration speed is much slower and as seen from Table 2, the average specific cake resistance is much higher compared to limed muds produced from Limes 1, 2B and 4.

Lime 2B and 4 originate from the same pulp mill, samples being taken at different instances. In causticizing experiments a much more smaller dose of lime was required to achieve both white liquor CE 70 % and 80 % when using Lime 4 compared to Lime 2B. This is due Lime 4 being more reactive by containing significantly less residual carbonate (0.86 %) compared to Lime 2B (2.42 % residual carbonate). Hence, Lime 4 causticizer slurry had a much lower solids content than causticizer slurry of Lime 2B.

The filtration plots for washed lime muds produced from all reburned lime samples (target CE 80 %) used in this study are shown in Figure 22 and filterability plots are shown in Figure 23.

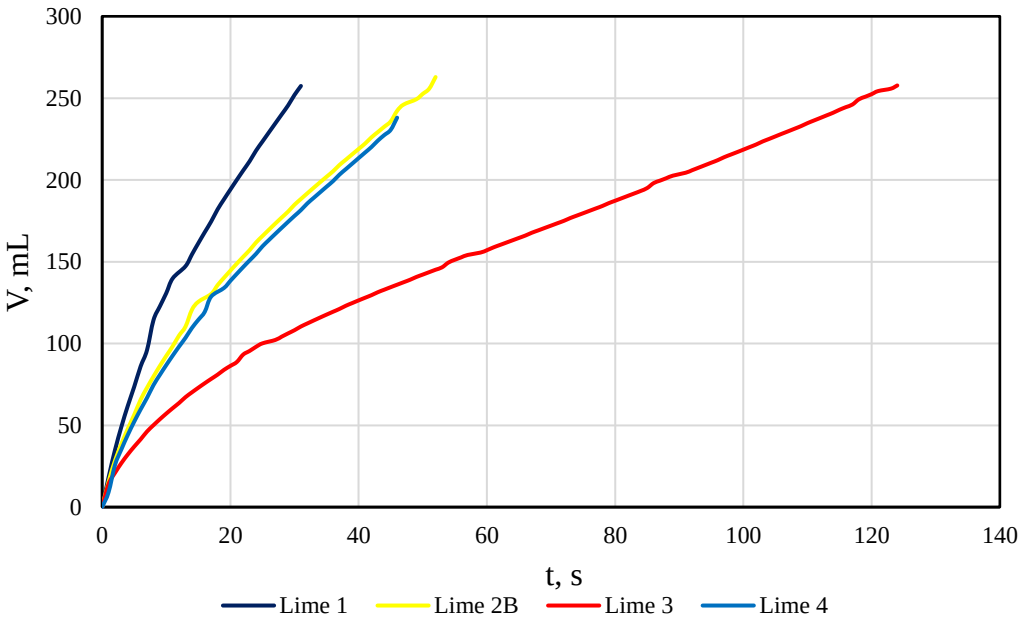

Figure 22 Washed lime mud filtration plot for all lime types. Target CE 80 % (TTA 180 g/L NaOH, 90 min reaction time)

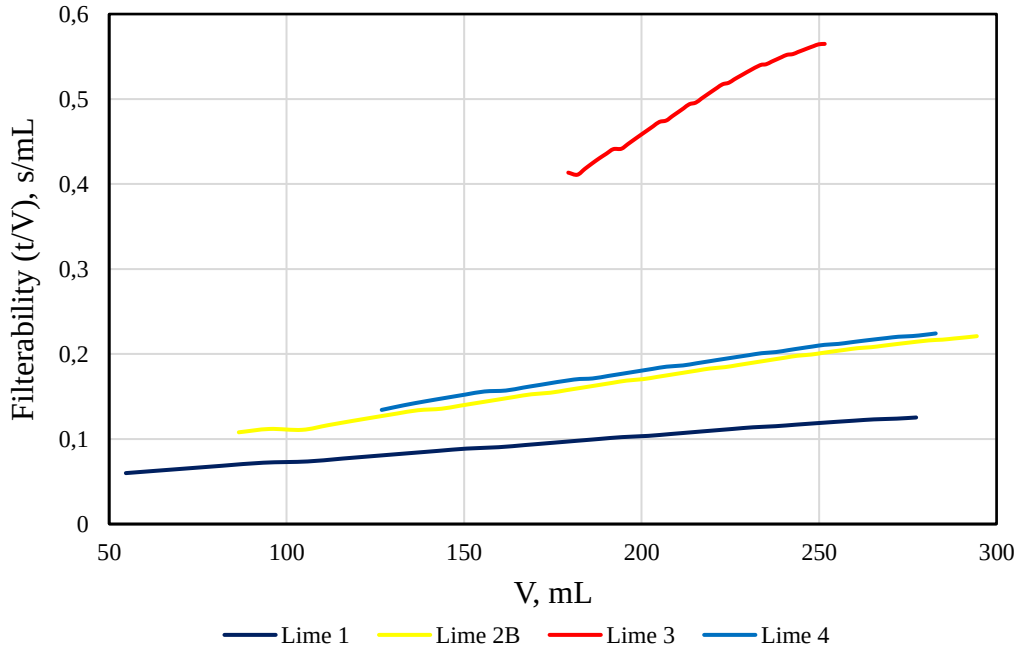

Figure 23 Washed lime mud filterability plot for all lime types. Target CE 80 % (TTA 180 g/L NaOH, 90 min reaction time)

As discussed in previous section, the effect of increased liming ratio on filtration properties persist in washed lime mud which is apparent for lime muds produced from all reburned lime samples used in this study. For washed lime muds, again lime mud produced from Lime 3 differs greatly in filtration performance compared to other lime mud samples.

The results of PSD analysis (average) are presented in Table 3.

Table 3 Results of PSD analysis (average). Notation "*CE*" refers to target CE % of white liquor during causticizing and notation "*L*" refers to lime used in causticizing.

Experiment	Dx (10), µm	Dx (50), µm	Dx (90), µm	D [4;3], µm	D [3;2], µm
CE70L1	4.69	16.85	38.45	19.50	6.67
CE80L1	6.24	18.65	36.50	20.40	7.27
CE85L1	4.00	13.70	26.55	14.80	5.08
CE70L2B	4.32	15.00	33.00	17.30	5.81
CE80L2B	4.47	16.00	32.00	17.70	6.15
CE85L2B	4.56	15.70	31.15	17.40	5.67
CE70L3	2.51	20.30	146.85	51.30	5.41
CE80L3	2.64	14.90	109.50	37.70	5.25
CE70L4	4.42	17.40	37.70	20.00	6.11
CE80L4	4.23	15.90	38.65	19.05	6.43

The average particle size across all lime mud samples are quite similar. Most notably, lime mud produced from Lime 3 contains both the smallest and the largest particles from the bunch. This could be due agglomeration of smaller particles during causticizing which interestingly did not occur for other lime types.

In Figure 24 the average specific cake resistance is plotted against Sauter diameter for all lime types at respective target CE %.

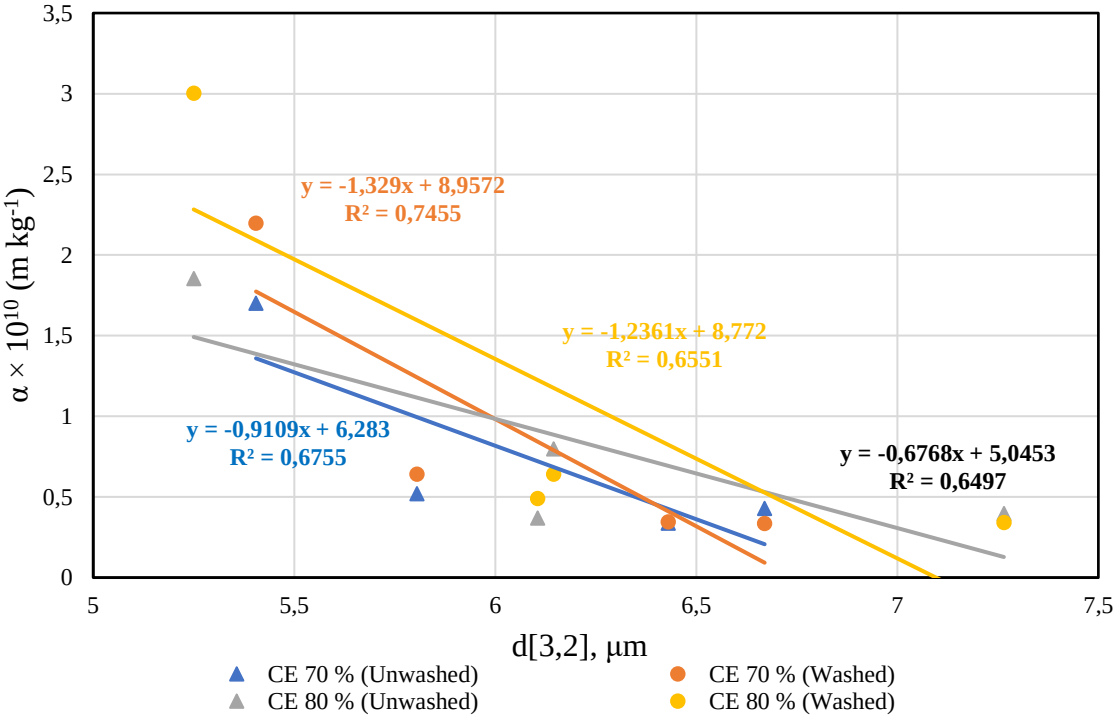

Figure 24 Average specific cake resistance plotted against particle size (Sauter diameter) at specific target CE % for all lime types.

Based on Figure 24, a mediocre correlation between lime particle size and average specific cake resistance exists. However, based on how the points are scattered in Figure 24 the linear correlation probably breaks if finer lime is used in causticizing. The particle size distributions of all lime mud samples were further investigated. The volume-based particle size distribution for all lime muds at their respective target CE % is shown in Figure 25.

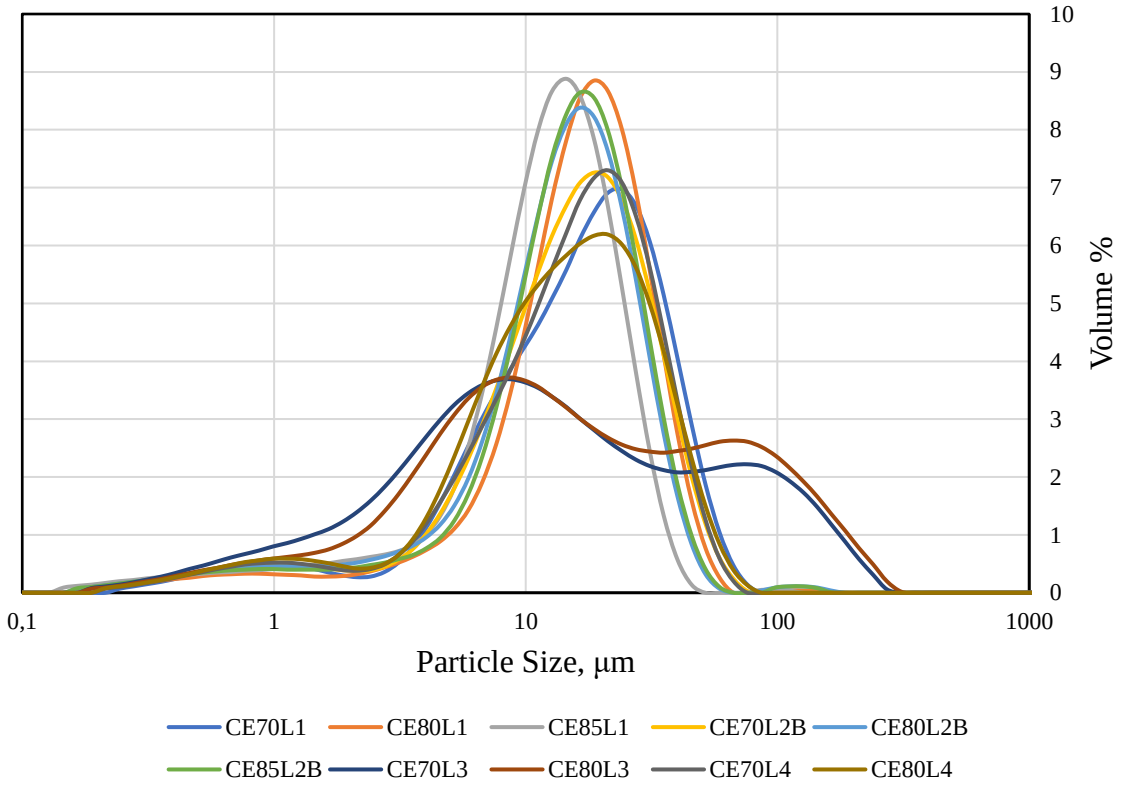

Figure 25 Volume based particle size distribution plot for all lime mud samples. "*CE*" notation refers to target causticizing degree and "*L*" notation refers to used lime in causticizing experiment.

The particle size distribution of Lime 3 is considerably wider compared to lime muds produced from Limes 1, 2B and 4. Reburned lime particle size is known to carry over to the produced lime mud, and it can be concluded that reburned limes 1, 2B and 4 are similar in particle size, Lime 3 consisting of much more smaller particles. As mentioned before, a wider particle size distribution leads to more densely packed filter cake which affects filtration performance. Additionally, lime mud produced from Lime 3 consist of considerably smaller particles which decrease both filtration and settling performance.

The morphology of lime mud particles was studied using scanning electron microscope (SEM). No distinct features in morphology of lime mud particles produced from different limes were observed. X-ray diffraction (XRD) analysis was only able to identify portlandite ($CaOH_2$) and pirssonite ($Na_2CO_3 \bullet CaCO_3 \bullet 2H_2O$) in both unwashed and washed lime mud samples.

Average specific cake porosity values plotted against zeta potential for lime muds produced from all reburned lime samples used in this study are shown in Figure 26.

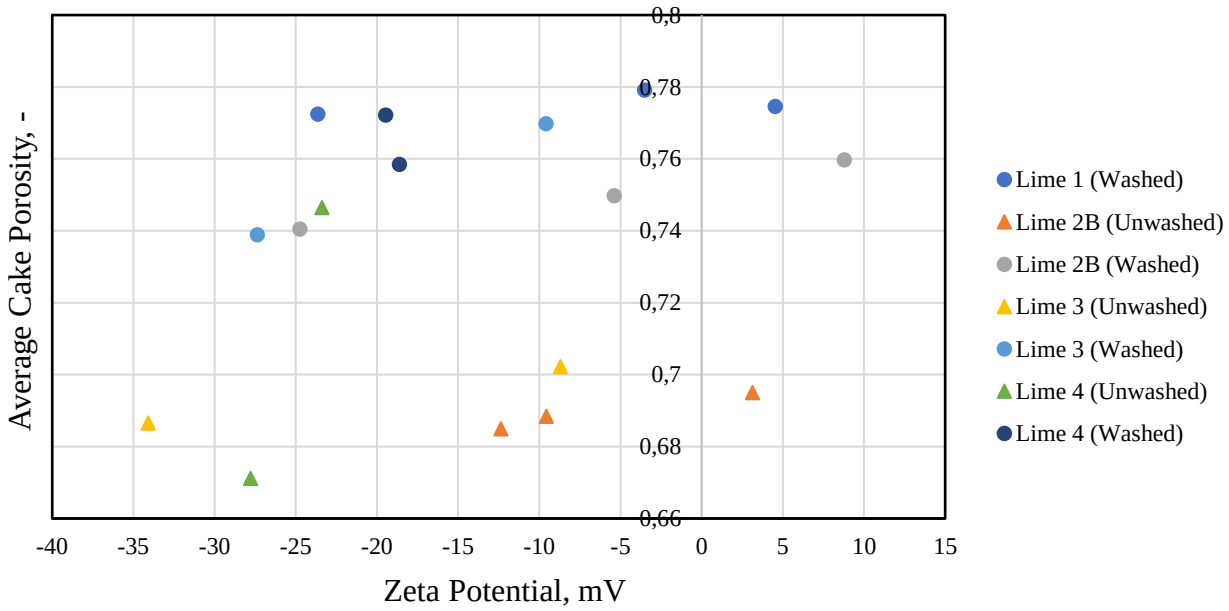

Figure 26 Average cake porosity (void volume fraction) of all lime types plotted against zeta potential for both unwashed and washed samples.

Generally, an increase in cake porosity as zeta potential increases can be seen for all lime mud samples except for unwashed lime mud produced from Lime 4. As mentioned before, the increase in cake porosity is due to increase in repulsive forces between the lime mud particles which results in more loosely packed filter cake and increased moisture content. Although, lime mud produced from Lime 3 has a considerably wider particle size distribution compared to other lime mud samples which in theory would result in more densely packed cake the results are conflicting. The cause of this phenomenon could be related to repulsive forces between the particles, as seen from elemental analysis results performed with ICP-MS in Table 1 the NPE contents in Lime 3 are substantially higher compared to other reburned lime samples.

Average moisture content values plotted against zeta potential for lime muds produced from all reburned lime samples used in this study are shown in Figure 27.

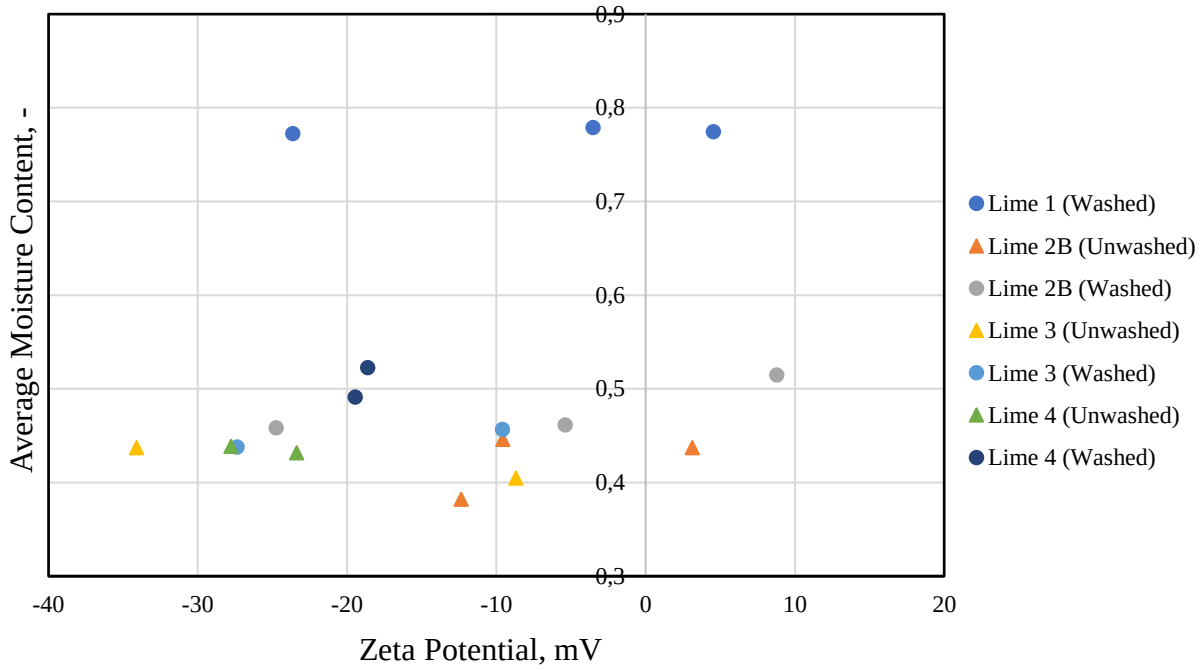

Figure 27 Average moisture content (moisture fraction) for all lime types plotted against zeta potential for both unwashed and washed samples.

Generally, the average moisture content within lime mud filter cake seems to increase as zeta potential becomes more positive. The increase of moisture content is especially visible for lime mud samples produced from Lime 2B. The moisture content of washed lime mud produced from Lime 1 is exceptionally high compared to other samples. The increase in repulsive forces between lime mud particles decreases filtration efficiency which explains higher moisture content in the filter cakes when zeta potential increases.

9.4 Lime mud zeta potential

Causticizing reactions were performed to target specific causticizing efficiencies (CE %) of white liquor representing different states of causticizing process. The target CE % values used in this study were:

- CE of 70 %, representing underlimed operating conditions
- CE of 80 %, representing normal operating conditions
- CE of 85 %, representing overlimed operating conditions.

It should be noted here that due to high alkalinity of the synthetic green liquor used, white liquor causticity of 85 % was not reached. In this study "*CE 85 %*" notation is used to note lime mud produced at overlimed conditions.

In previous studies overliming was found to increase lime mud zeta potential to increasingly more positive values. This observation was confirmed in this study, as seen from Figure 28 in which lime mud zeta potential is plotted against liming ratio for both unwashed and washed samples.

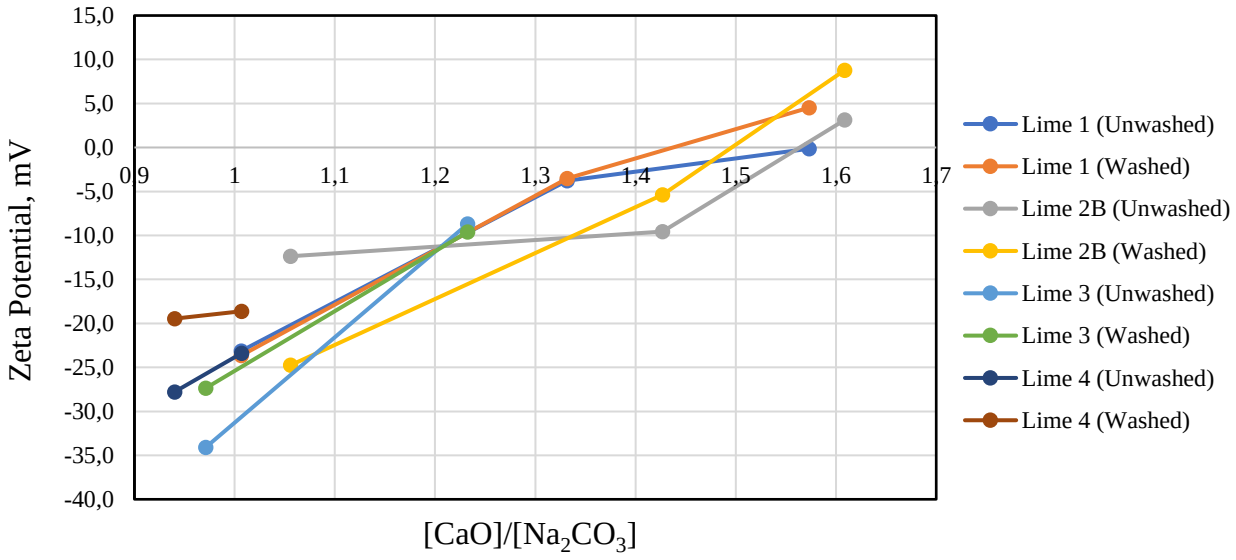

Figure 28 The effect of liming ratio on lime mud zeta potential for both unwashed and washed samples.

Zeta potential of washed lime mud samples were higher compared to their unwashed counterparts. Alkalinity is known to change calcite zeta potential to increasingly negative values and the washing step had probably removed negative ionic species from crystal

lattice. Although, free lime is more soluble to water than in alkaline which in theory could decrease zeta potential, in this study such effect was not observed.

As discussed in Section 6.5, the increase in lime mud zeta potential is due to formation of free lime. The free lime content within lime mud samples were determined using thermogravimetric analysis (TGA). In Table 4, the free lime contents within both unwashed and washed lime mud samples are summarized. The Mg contents analyzed by ICP-MS were taken into account since 1 wt-% of $Mg(OH)_2$ increases perceived free lime content by 1.3 wt-%.

Table 4 Free lime contents for both unwashed and washed lime mud samples. Mg content in reburned limes has been taken into account.

Lime Type	**CE, %**	**Unwashed $Ca(OH)_2$, wt-%**	**Washed $Ca(OH)_2$, wt-%**
Lime 1	70	3,00	2,68
	80	4,56	3,75
	85	7,30	6,14
Lime 2B	70	3,79	2,82
	80	5,54	4,06
	85	6,47	5,36
Lime 3	70	2,82	1,29
	80	4,22	2,82
Lime 4	70	3,26	2,14
	80	3,48	2,23

The correction for Mg content was based on two assumptions;

1) All Mg in the reburned lime will react with water forming $Mg(OH)_2$
2) Due to very low solubility of $Mg(OH)_2$ to water, $Mg(OH)_2$ was treated insoluble in calculations.

As seen from Table 4, the washing technique used in this study removed some of the free lime. However, the free lime content within the washed samples increased as liming ratio increased. Based on these results, lime mud washing has a negligible effect of lime mud zeta potential and zeta potential measurement could be performed on washed lime mud in pulp mills.

In Figure 29, the correlation between liming ratio and formation of free lime is visually presented. In Figure 30 lime mud zeta potential is plotted against free lime content measured within the lime mud sample.

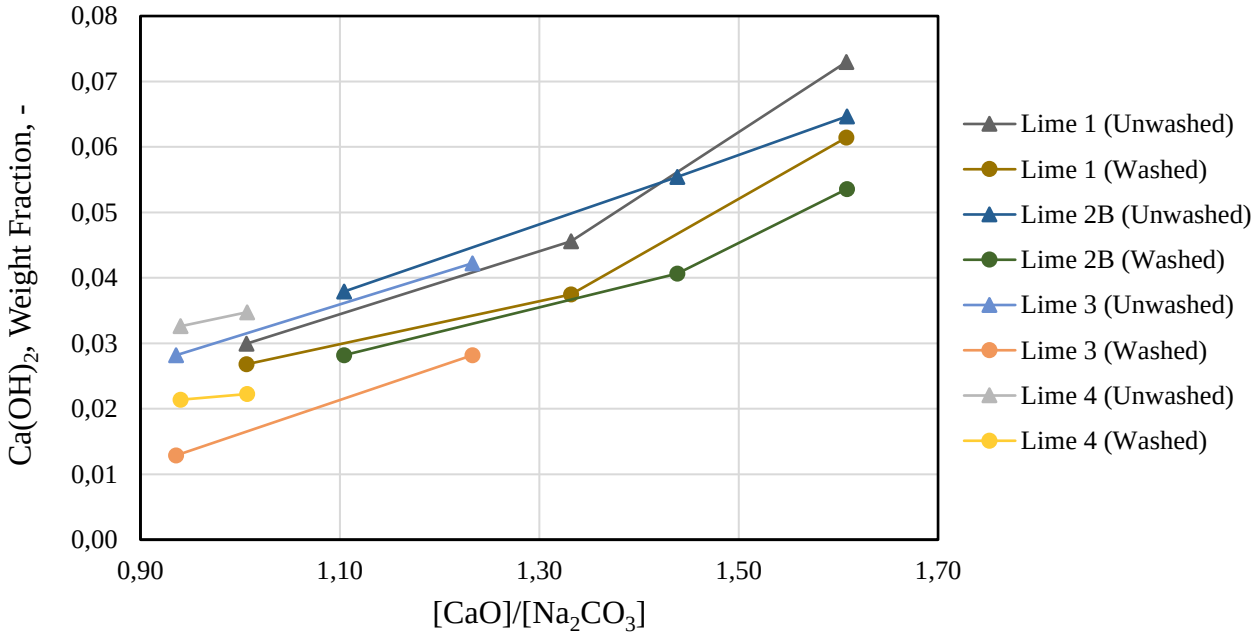

Figure 29 The impact of increasing liming ratio on formation of free lime visualized for both unwashed and washed lime mud samples.

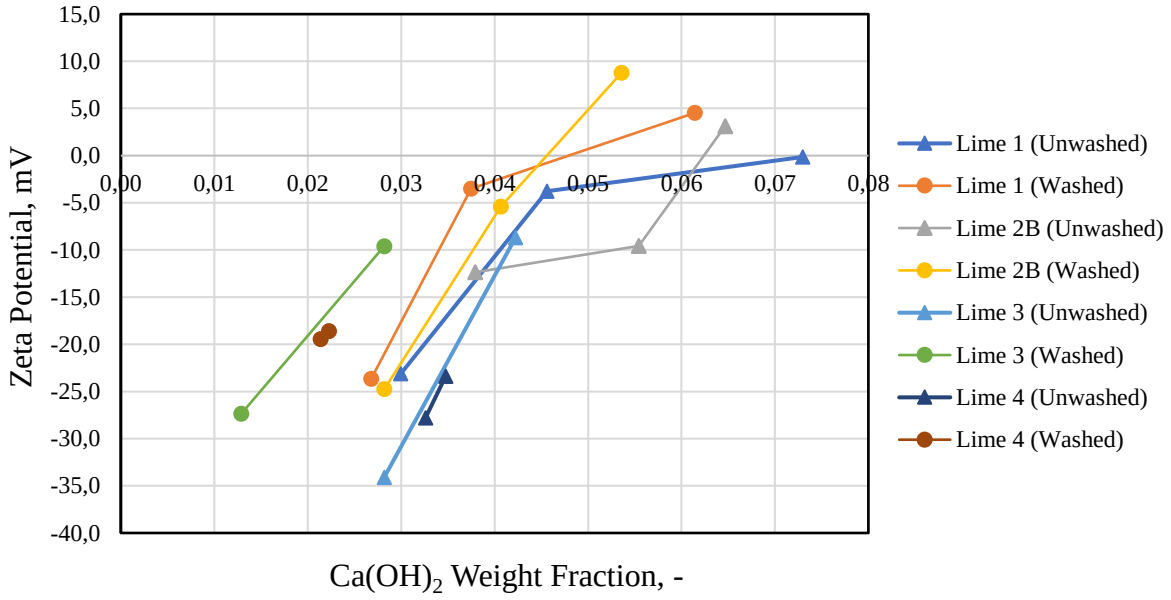

Figure 30 The impact of increased free lime content on lime mud zeta potential for both unwashed and washed lime mud samples.

The increase of free lime content with increasing liming ratio seems to be linear based on the data gathered in this study. The effect of washing step to free lime content can be clearly seen from Figure 29 as measured free lime values being plotted lower compared to their unwashed counterparts. In Figure 30, the effect of increased free lime content to the lime mud zeta potential can be clearly visualized.

9.5 Lime mud streaming potential

Streaming potential of lime mud samples were additionally measured. This was done to study if a similar correlation to zeta potential exists between liming ratio and streaming potential. If such a correlation would exist, an alternative method with less extensive sample preparation could be considered. Fiber potential analyzers are already quite common in pulp mills and the measurement technique is based on measuring streaming potential. It should be noted that the methodology of streaming potential measurement in this study was quite crude and it is suggested to perceive the results with caution.

The results of streaming potential measurements for lime mud samples produced from Lime 2B are presented in Table 5.

Table 5 Results of streaming potential measurements for lime mud samples produced from Lime 2B. Notation "*CE*" refers to target CE % of white liquor in causticizing and notation "*L*" refers to lime used.

Experiment	Conductivity, mS/cm	Streaming Potential, mV	Zeta Potential, mV (Zetasizer)	Zeta Potential, mV (FPA touch!)
CE70L2B	9.76	-0.10	-27.6	-0.53
CE70L2B	17.62	-0.05		-0.45
CE80L2B	15.11	0.26	-14.41	1.97
CE80L2B	16.98	0.22		1.93
CE85L2B	15.28	0.16	-0.66	1.23

Measurements were performed for both native samples and samples with constant conductivity. Conductivity was adjusted by using white liquor from causticizing. At underlimed conditions, both zeta and streaming potentials acquire negative values. Based on results by previous authors and results in this study, streaming potential was thought to increase as liming ratio increased. However, this was not observed and streaming potential at "normal" operating condition was measured to be higher than in overlimed condition.

The conductivity of sample solutions was high, even exceeding the sample requirements of the used equipment (10 mS/cm). Further measurements of samples at target CE of 80 % and 85 % were done to study if solution conductivity was the key factor. The results are presented in Table 6.

Table 6 Results of streaming potential measurements for lime mud samples produced from Lime 2B. Notation "*CE*" refers to target CE % of white liquor in causticizing and notation "*L*" refers to lime used.

Experiment	Conductivity, mS/cm	Streaming Potential, mV	Zeta Potential, mV (Zetasizer)	Zeta Potential, mV (FPA touch!)
CE80L2B	11.41	0.34	-14.41	2.06
CE80L2B	8.72	0.52		2.27
CE85L2B	9.24	0.51	-0.66	2.33

As seen from the results presented in Table 6, even at acceptable level of solution conductivity the streaming potential values for both, at normal and overlimed conditions are almost identical. Based on these results it can be concluded that the streaming potential measurement method is unable to be used to detect overliming.

10 Conclusions

Overliming in causticizing is known to cause various operating problems throughout pulp mill. The most notable operating problems are linked to increased free lime contents within lime mud which affect the lime mud settling and filtration properties negatively. [2] Decrease in settling and filtration properties are linked to increased lime kiln fuel usage, precoat filter plugging and lime kiln ring formation. [3,4] Currently the amount of free lime is measured using thermal decomposition or NH_4Cl methods, latter being conducted as unsuitable to determine free lime content in lime mud [40]. In previous studies, a novel concept was discovered linking liming ratio and lime mud zeta potential. Zeta potential was found to be an effective way to evaluate lime mud settling and filtration properties. [28]

The objective of the master's thesis was to study findings in previous studies, the effect of lime mud washing and evaluate the applicability of streaming potential measurement as an alternative method in lime mud evaluation. Causticizing experiments were performed using synthetic green liquor and using lime samples gathered from Finnish pulp mills. Liming ratio in causticizing was varied to produce lime mud representing the causticizing process in different process states. The process states are represented by target causticizing efficiency (CE %) of white liquor, 70 % representing underlimed, 80 % representing normal and 85 % representing overlimed operating conditions. Lime muds produced from causticizing experiments were used in settling and filtration tests and both zeta and streaming potential were measured.

Findings from previous studies were confirmed; lime mud settling and filtration rates decreased as liming ratio increased. The phenomenon was present for all lime mud samples produced from all reburned lime samples used in this study. The decreased settling and filtration rates are caused by an increase in repulsive forces between lime mud particles when lime mud zeta potential increases. No correlation between lime mud particle size and settling velocity was found in this study and, a moderate but apparently nonlinear correlation between lime mud particle size and lime mud filterability was confirmed.

Increased liming ratio was confirmed to increase free lime content within lime mud samples. The cause for increase in lime mud zeta potential is due to free lime; Ca^{2+} concentration is known to make calcite zeta potential more positive. At underlimed conditions the effect of CO_3^{2-} ions decrease lime mud zeta potential which can be seen as increasingly negative zeta

potential values. The effect of lime mud washing on zeta potential was studied by making a 10 wt-% slurry on which filtration test were performed and zeta potential was measured. Although $Ca(OH)_2$ is more soluble in water than in alkali the decreased filtration rates caused by overliming were carried over to the washed lime mud and a negligible effect on lime mud zeta potential was observed. Based on these results, zeta potential measurements could be performed on washed lime mud. Confirming results from previous studies ensures a possibility utilizing online measurement technique to detect overliming if suitable equipment would be built.

Streaming potential measurements were performed on lime mud samples to evaluate applicability of streaming potential as a mean to detect overliming. Although streaming potential was observed to have a negative value at underlimed conditions, the results at normal and overlimed conditions were found to be identical. However, the methods used in this study for evaluation of streaming potential to detect overliming were crude. A more rigorous study should be done before drawing any final conclusions.

Polyvalent ions may affect calcite zeta potential, hence lime muds, and Mg^{2+} ions are known to behave identically to Ca^{2+} ions regarding calcite zeta potential. Although in this study non-process elements (NPEs) found within the reburned lime samples did not exhibit any noticeable effect regarding the zeta potential, a more rigorous study should take be performed regarding the effect of NPEs on lime mud zeta potential.

Appendix list

References

[1] Biermann, C. J. (1996). “Handbook of pulping and papermaking,” Second edition, San Diego: Academic Press.

[2] Campbell, A. J. (1985). “Effects of Lime Quality and Dosage on Causticizing and Lime Mud Settling Properties,” *Pulp & Paper Canada*, pp. 67-71.

[3] Santos, S., Tran, H. (2008). “Experience of low lime mud solids problems at a kraft pulp mill,” *O'Papel, 69*(6), pp. 69-79.

[4] Tikka, P. (2008). “Papermaking science and technology: Book 6, Chemical pulping. Part 2, Recovery of chemicals and energy,*”* (Second edition). Helsinki: *Finnish Paper Engineers' Association* : Paperi ja puu.

[5] Ek, M., Gellerstedt, G., Henriksson, G. (2009). “Pulp and paper chemistry and technology: Volume 2, Pulping chemistry and technology,” Berlin: Walter de Gruyter.

[6] Crittenden, J. C., Howe, K. J., Hand, D. W., Tchobanoglous, G., Trussell, R. R. (2012). “Principles of water treatment,” Third edition, Student edition. Hoboken, New Jersey: John Wiley & Sons, Inc.

[7] Rushton, A., Ward, A. S., Holdich, R. G. (2000). “Solid-liquid filtration and separation technology,” Second edition. Weinheim: Wiley-VCH.

[8] Svarovsky, L. (2000). “Solid-liquid separation,” Fourth edition. Oxford: Butterworth Heinemann.

[9] Kinnarinen, T., Tuunila, R., Häkkinen, A. (2017). “Reduction of the width of particle size distribution to improve pressure filtration properties of slurries,” *Miner. Eng.*, vol. 102, pp. 68–74.

[10] Dorris, G. M. (1993). “The Physical Characterization of Hydrated Reburned Lime and Lime Mud Particles,” Journal of Pulp and Paper Science, pp. 256-267.

[11] Lindblom, J., Hanson, C., Theliander, H. (1996). “Sintering of calcinated lime mud - The influence of carbon dioxide: Carbon dioxide strongly increases the sintering rate,” *Pulp and Paper Canada*, pp. 45-50.

[12] Dorris, G. M., Allen, L. H. (1985). “Effect of Reburned Lime Structure on the Rates of Slaking, Causticizing and Lime Mud Settling,” *Journal of Pulp and Paper Science*, pp. 89-97.

[13] Tran, H. “Lime kiln chemistry and effects of kiln operations,” pp. 1-9.

[14] Commandré, J. M., Salvador, S., Nzihou, A. (2007). “Reactivity of Laboratory and Industrial Limes,” *Chem. Eng. Res. Des.*, vol. 85, no. 4, pp. 473–480.

[15] Weiner, B. B., Tscharnuter, W.W., Fairhurst, D. “Zeta Potential: A New Approach,” pp. 1-12.

[16] Wakeman, R. (2007). “The influence of particle properties on filtration,” *Sep. Purif. Technol.*, vol. 58, no. 2, pp. 234–241.

[17] Zeta-Meter Inc., “Zeta Potential: A Complete Course in 5 Minutes”.

[18] Sun, D. (2016). “Effect of Zeta Potential and Particle Size on the Stability of SiO_2 Nanospheres as Carrier for Ultrasound Imaging Contrast Agents,” *Int. J. Electrochem. Sci.*, pp. 8520–8529.

[19] Cruz, R. C. D., Segadães, A. M., Oberacker, R., Hoffmann, M. J. (2017) “Double layer electrical conductivity as a stability criterion for concentrated colloidal suspensions,” *Colloids Surf. Physicochem. Eng. Asp.*, vol. 520, pp. 9–16.

[20] Butt, H. J., Kappl, M. (2018). ”Surface and Interfacial Forces,” Second edition. John Wiley & Sons.

[21] Al Mahrouqi, D., Vinogradov, J., Jackson, M. D. (2017) “Zeta potential of artificial and natural calcite in aqueous solution,” *Adv. Colloid Interface Sci.*, vol. 240, pp. 60–76.

[22] Saini, R., Kenny, M., Barz, D. P. J. (2015). “Electroosmotic flow through packed beds of granular materials,” *Microfluid. Nanofluidics*, vol. 19, no. 3, pp. 693–708.

[23] Koutsoukos, P. K., Klepetanis, P. G., Spanos, N. (2015) “Calculation of Zeta Potentials from Electrokinetic Data,” *Encyclopedia of Surface and Colloid Science*, pp. 1097-1112.

[24] Madsen, L. (2015). "Calcite: Surface Charge," *Encyclopedia of Surface and Colloid Science*, pp. 1084-1096.

[25] Alroudhan, A., Vinogradov, J., Jackson, M. D. (2016). "Zeta potential of intact natural limestone: Impact of potential-determining ions Ca, Mg and SO_4," *Colloids Surf. Physicochem. Eng. Asp.*, vol. 493, pp. 83–98.

[26] Li, S., Leroy, P., Heberling, F., Devau, N., Jougnot, D., Chiaberge, C. (2016). "Influence of surface conductivity on the apparent zeta potential of calcite," *J. Colloid Interface Sci.*, vol. 468, pp. 262–275.

[27] Song, J., Zeng, Y., Wang, L., Duan, X., Puerto, M., Chapman, W. (2019). "Surface complexation modeling of calcite zeta potential measurements in brines with mixed potential determining ions (Ca^{2+}, CO_3^{2-}, Mg^{2+}, SO_4^{2-}) for characterizing carbonate wettability".

[28] Azgomi, F. (2014). "Impact of Liming Ratio on Lime Mud Settling and Filterability in the Kraft Recovery Process".

[29] Poykio, R., Dahl, O., Nurmesniemi, H., Watkins, G. (2015). "Chemical fractionation of NPEs in slaker grits for environmental risks assessment," *J. Environ. Occup. Sci.*, vol. 4, no. 1, p. 22.

[30] Manskinen, K., Nurmesniemi, H., Poykio, R. (2011). "Total and extractable non-process elements in green liquor dregs from the chemical recovery circuit of a semi-chemical pulp mill," *Chem. Eng. J.*, vol. 166, no. 3, pp. 954–961.

[31] Salmenoja, K., Poukka, O., Battegazorre, M. (2009). "Management of non-process elements in Eucalyptus kraft pulps mills," *ABTCP*.

[32] Paleologou, M., Berry, R. M., Thompson, R., Jemaa, N. (1999). "Non-process elements in the kraft recovery cycle, Part II: control and removal options – A look at some of the new technologies available," *Pulp & Paper Canada, 101(2)*, pp. 47-51.

[33] Tran, H. N., Vakkilainen, E. K. (2007). "Advances in the Kraft Chemical Recovery Process," *The 3rd International Colloquium on Eucalyptus Pulp*, Belo, Horizonte, Brazil.

[34] Taylor, K. & Mcguffie, B. (2007). “Investigation of non-process element chemistry at Elk Falls mill - Green liquor clarifier and lime cycle,” *Pulp and Paper Canada*, *108*(2), pp. 27-32.

[35] Taylor, K., Bossons, D. (2006). “Investigation of green lime mud at Harmac mill,” *Pulp and Paper Canada*, 107(3), pp. 37-40.

[36] Lundqvist, P. (2009). “Mass and energy balances over the lime kiln in a kraft pulp mill”.

[37] Bjork, M., Engstrom, I. (2002). “Handling of non-process elements for improved runnability and reduced environmental impact,” *Pulp & Paper Canada*, *103(4)*, pp. 40-43.

[38] Scandinavian Pulp, Paper and Board Testing Committee, (1985). “White and green liquors – Total, active and effective alkali – Potentiometric titration*”*.

[39] Malvern Panalytical (2009). “Zetasizer Nano User Manual”.

[40] Mao, X., Ren, W., Tran, H. (2015). “Measurement of free lime content in lime mud,” *Tappi Journal*, 14(7), 481-489.

Lime dosage in causticizing experiments, corresponding liming ratio and measured causticizing efficiency (CE %) of produced white liquor are shown in Table 7. Initially theoretical amount of lime was calculated based on definition of CE % which most of the time resulted lower amount of lime than required. In this study average value of white liquor CE % between experiment repetitions were used when plotting figures.

Table 7 Lime usage in causticizing experiments and measured causticizing degree (CE %) of resulted white liquor. Notation "*CE*" refers to the target CE % of white liquor and "*L*" refers to lime used in causticizing.

Experiment	m(CaO), g	[CaO]/[Na_2CO_3], -	CE, %
CE70L1(1)	30.10	1.007	70.66
CE70L1(2)	30.08	1.006	72.28
CE80L1(1)	39.80	1.332	81.31
CE85L1(1)	45.99	1.539	80.30
CE85L1(2)	48.06	1.608	79.86
CE70L2B(1)	30.11	1.007	66.58
CE70L2B(2)	33.01	1.104	71.72
CE80L2B(1)	42.29	1.415	78.45
CE80L2B(2)	43.00	1.439	79.65
CE85L2B(1)	48.08	1.609	79.88
CE85L2B(2)	48.08	1.609	79.93
CE70L3(1)	30.08	1.006	75.38
CE70L3(2)	27.97	0.936	72.19
CE80L3(1)	36.83	1.232	79.85
CE80L3(2)	36.85	1.233	81.87
CE70L4(1)	28.10	0.940	70.63
CE70L4(2)	28.10	0.940	72.10
CE80L4(1)	30.10	1.007	80.84
CE80L4(2)	30.10	1.007	76.85

Filtration plots for unwashed lime mud samples produced from Lime 1 are shown in Figure 31 and filterability plots in Figure 32, and for washed lime mud samples in Figure 33 and in Figure 34 at respective target CE % values.

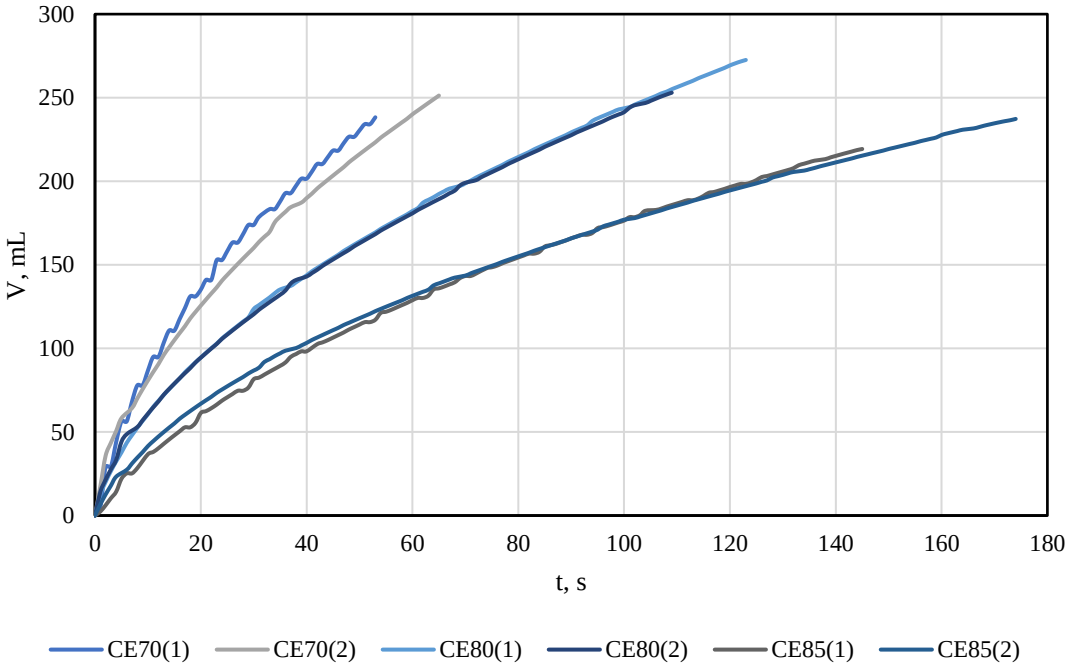

Figure 31 Filtration plots for unwashed lime mud samples produced from Lime 1 (target CE 70-85 %).

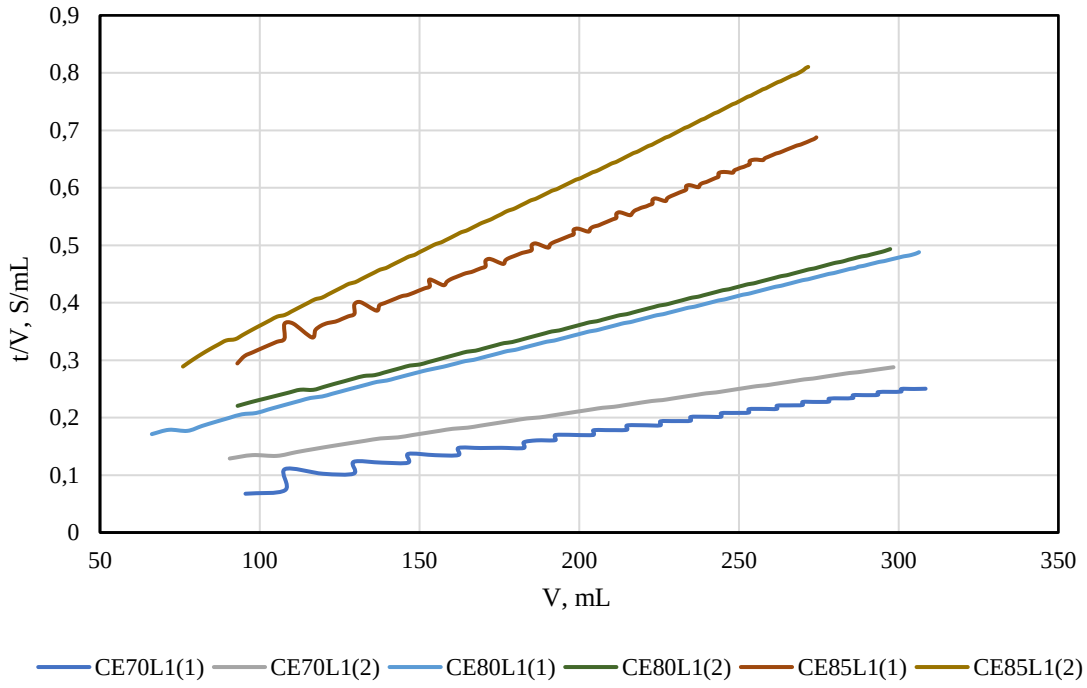

Figure 32 Filterability plots for unwashed lime mud samples produced from Lime 1 (target CE 70-85 %).

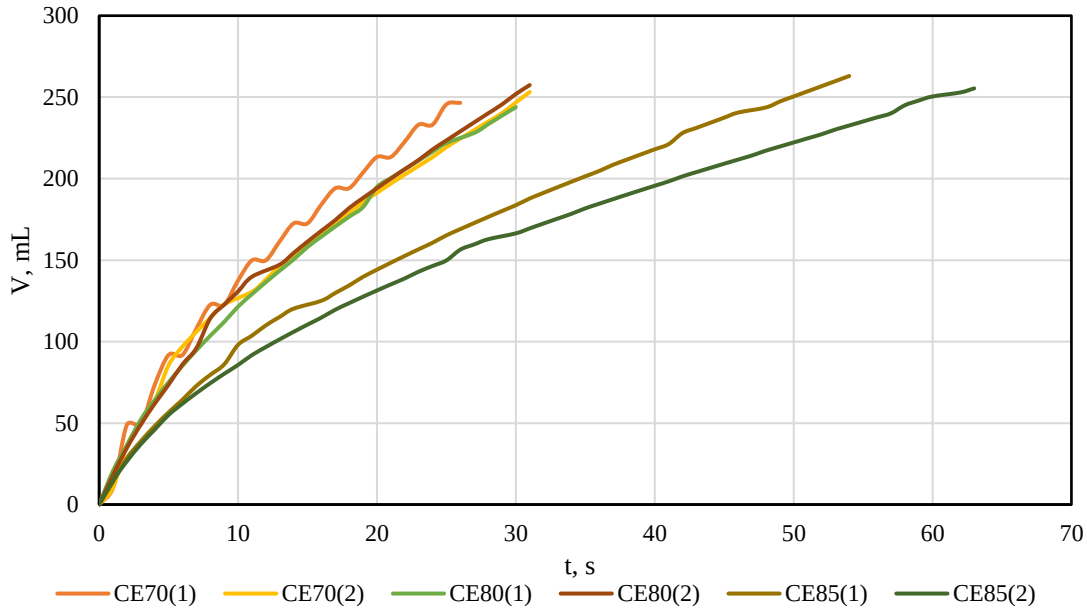

Figure 33 Filtration plots for washed lime mud samples produced from Lime 1 (target CE 70-85 %).

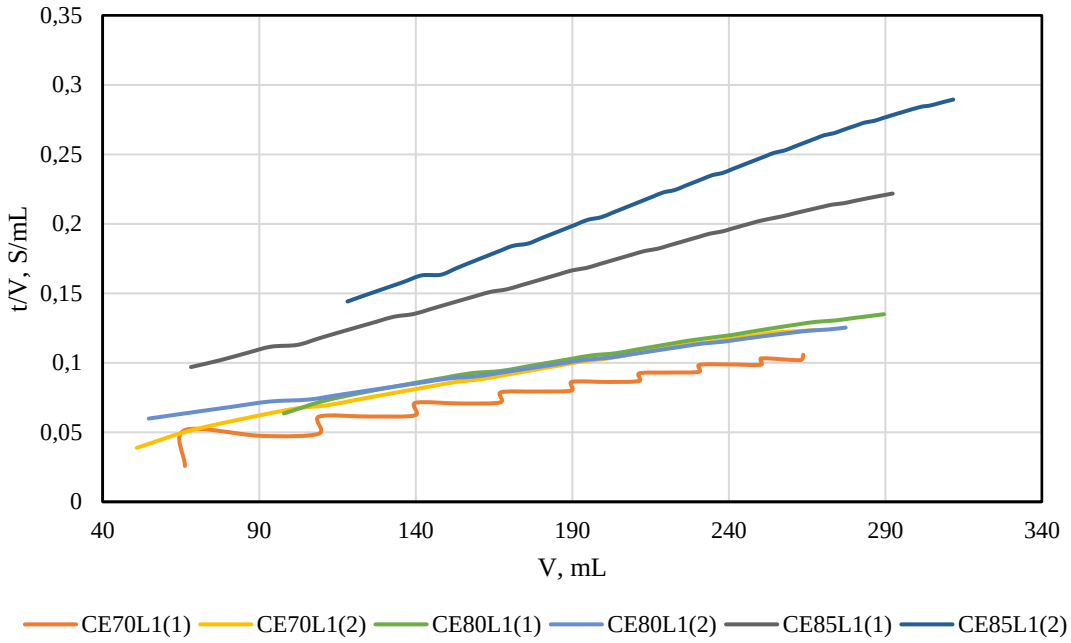

Figure 34 Filterability plots for washed lime mud samples produced from Lime 1 (target CE 70-85 %).

Filtration plots for unwashed lime mud samples produced from Lime 2B are shown in Figure 35 and filterability plots in Figure 36, and for washed lime mud samples in Figure 37 and in Figure 38 at respective target CE % values.

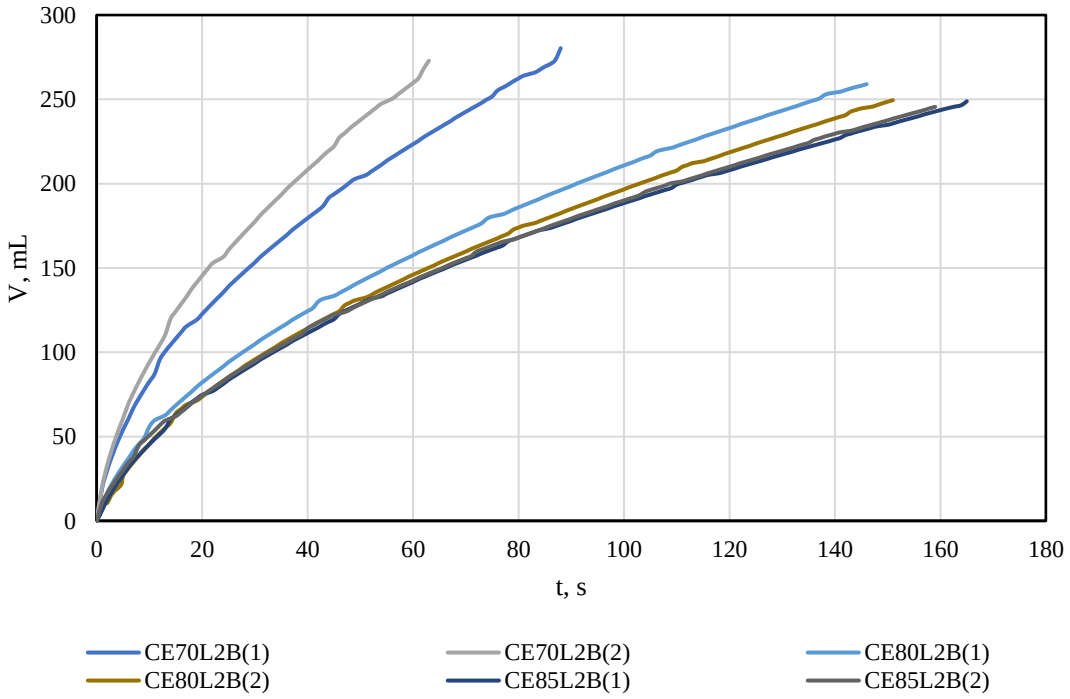

Figure 35 Filtration plots for unwashed lime mud samples produced from Lime 2B (target CE 70-85 %).

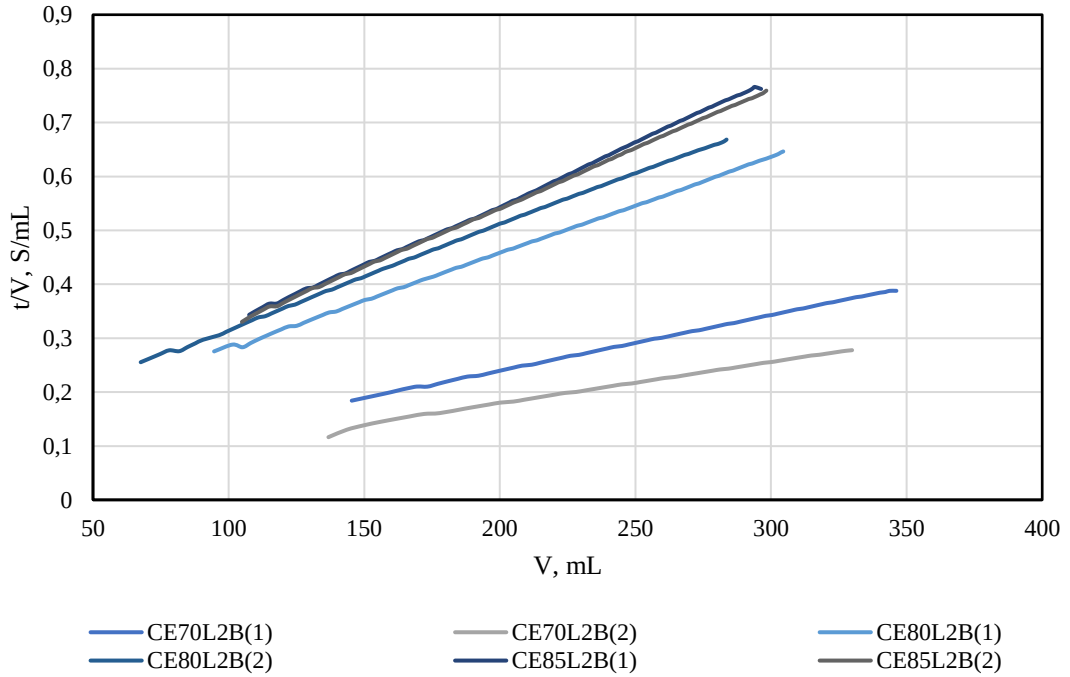

Figure 36 Filterability plots for unwashed lime mud samples produced from Lime 2B (target CE 70-85 %).

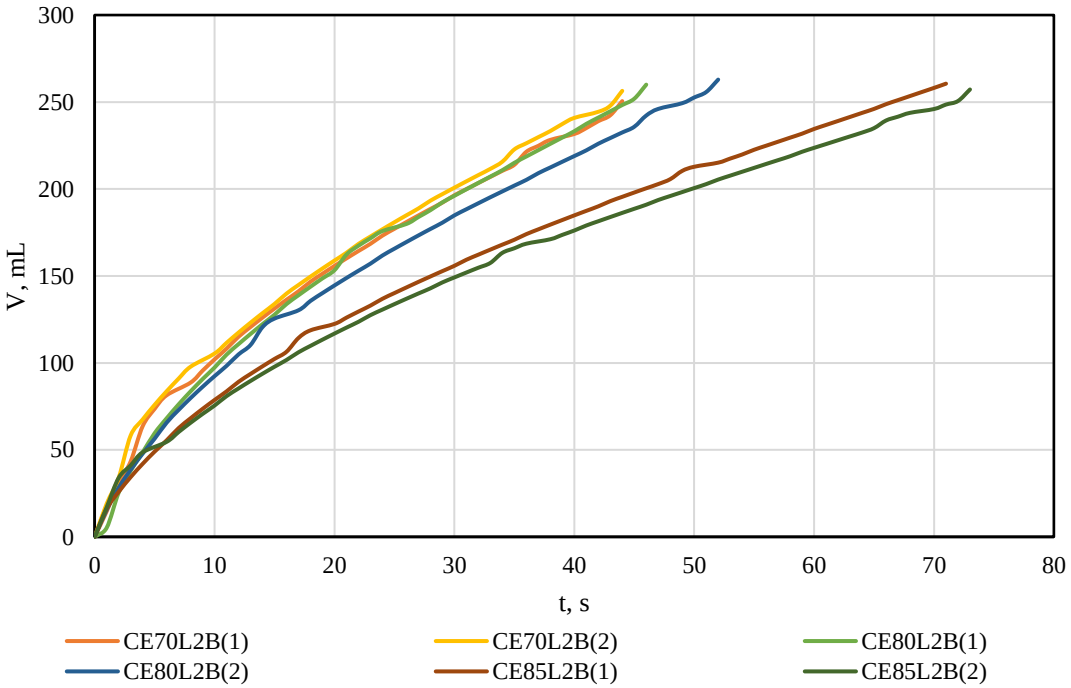

Figure 37 Filtration plots for washed lime mud samples produced from Lime 2B (target CE 70-85 %).

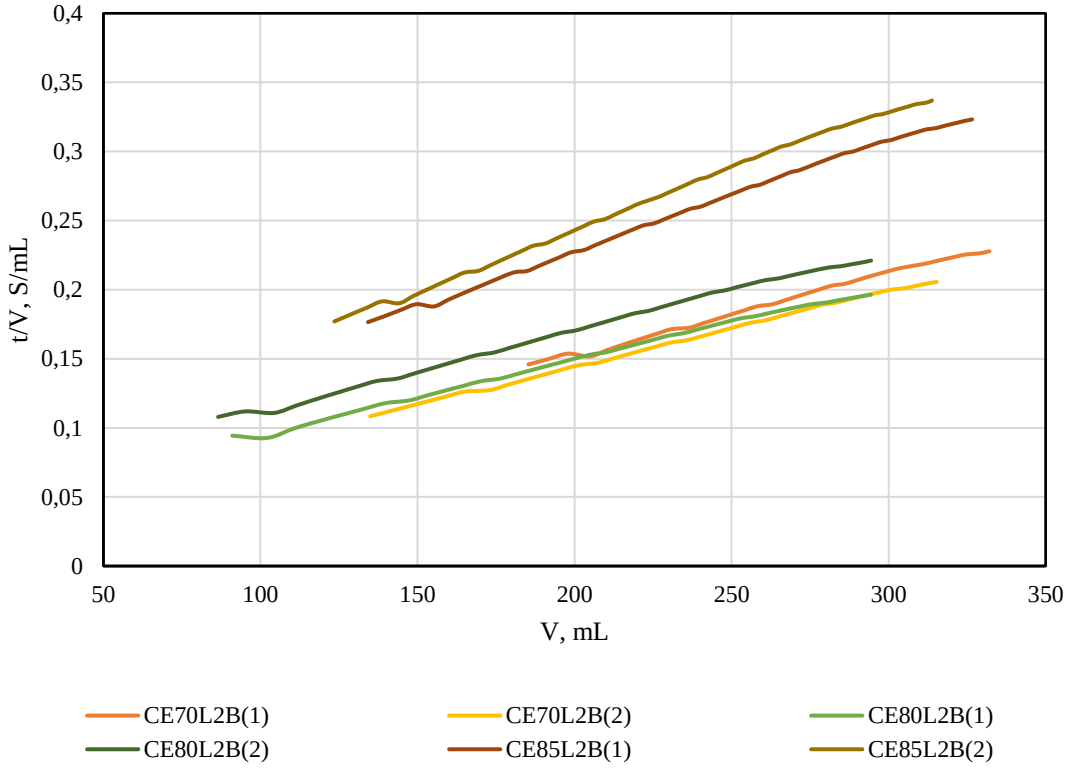

Figure 38 Filterability plots for washed lime mud samples produced from Lime 2B (target CE 70-85 %).

Filtration plots for unwashed lime mud samples produced from Lime 3 are shown in Figure 39 and filterability plots in Figure 40, and for washed lime mud samples in Figure 41 and in Figure 42 at respective target CE % values.

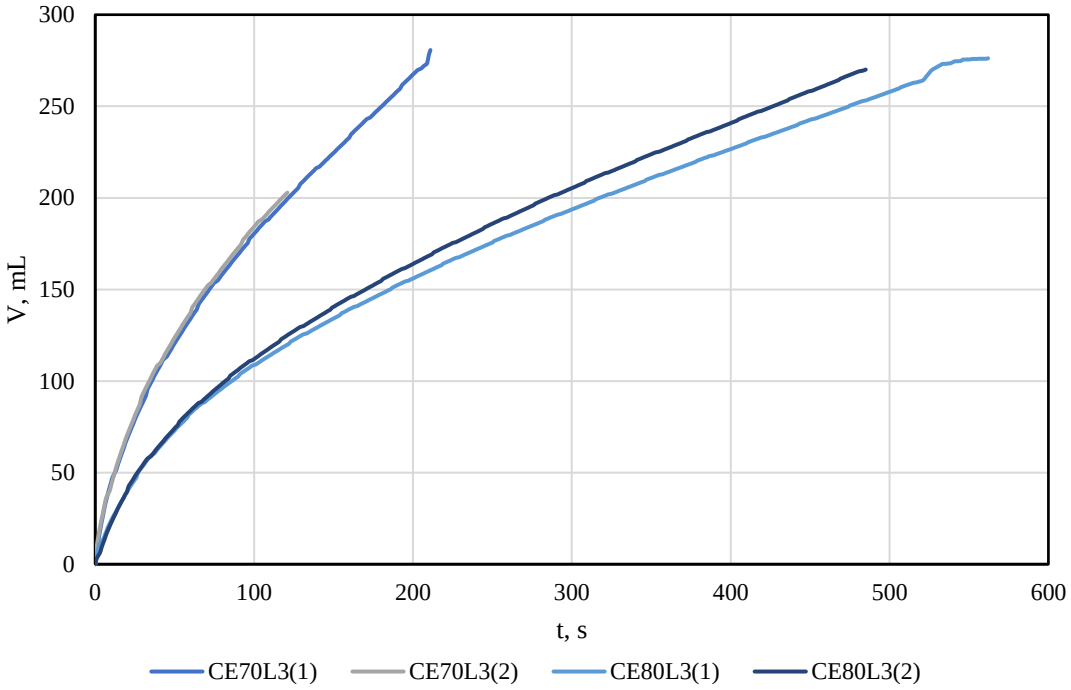

Figure 39 Filtration plots for unwashed lime mud samples produced from Lime 3 (target CE 70 and 80 %).

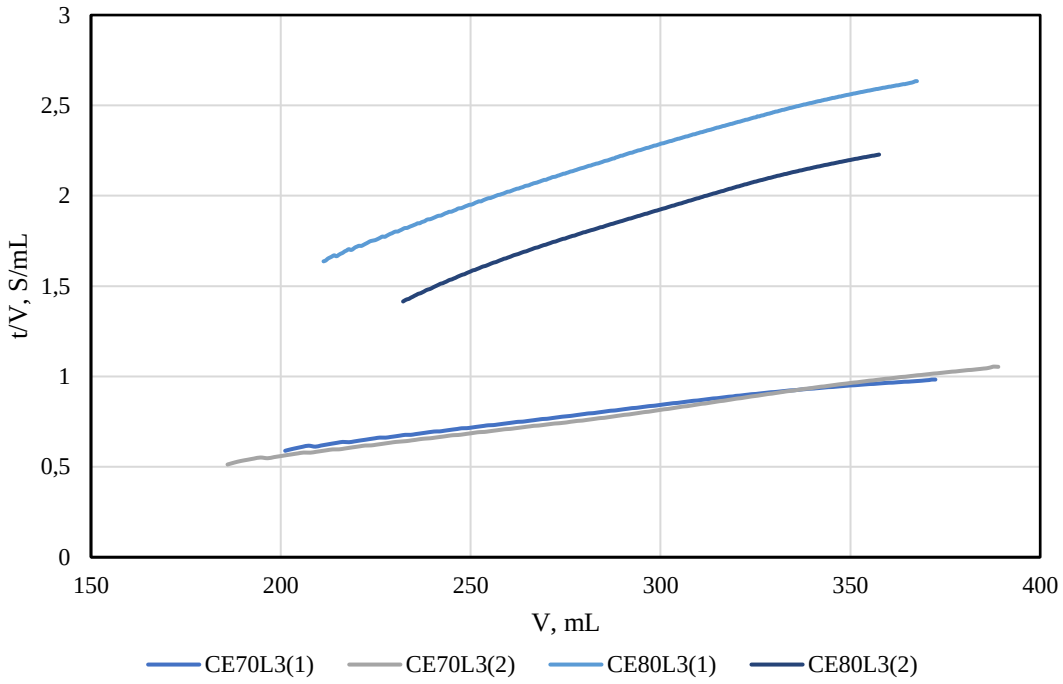

Figure 40 Filterability plots for unwashed lime mud samples produced from Lime 3 (target CE 70 and 80 %).

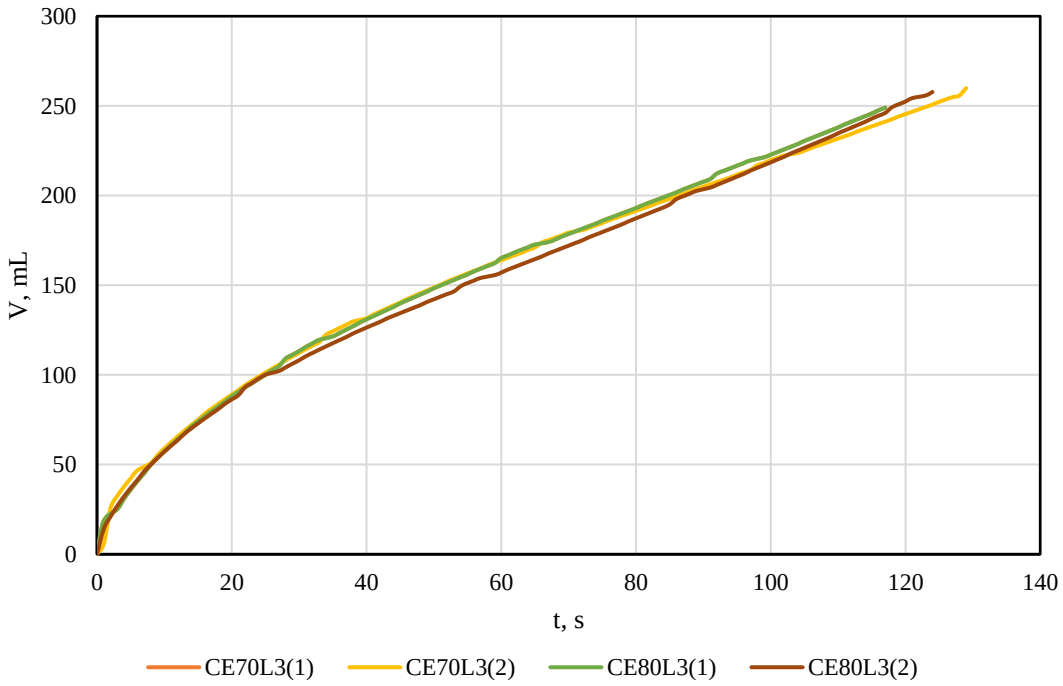

Figure 41 Filtration plots for washed lime mud samples produced from Lime 3 (target CE 70 and 80 %).

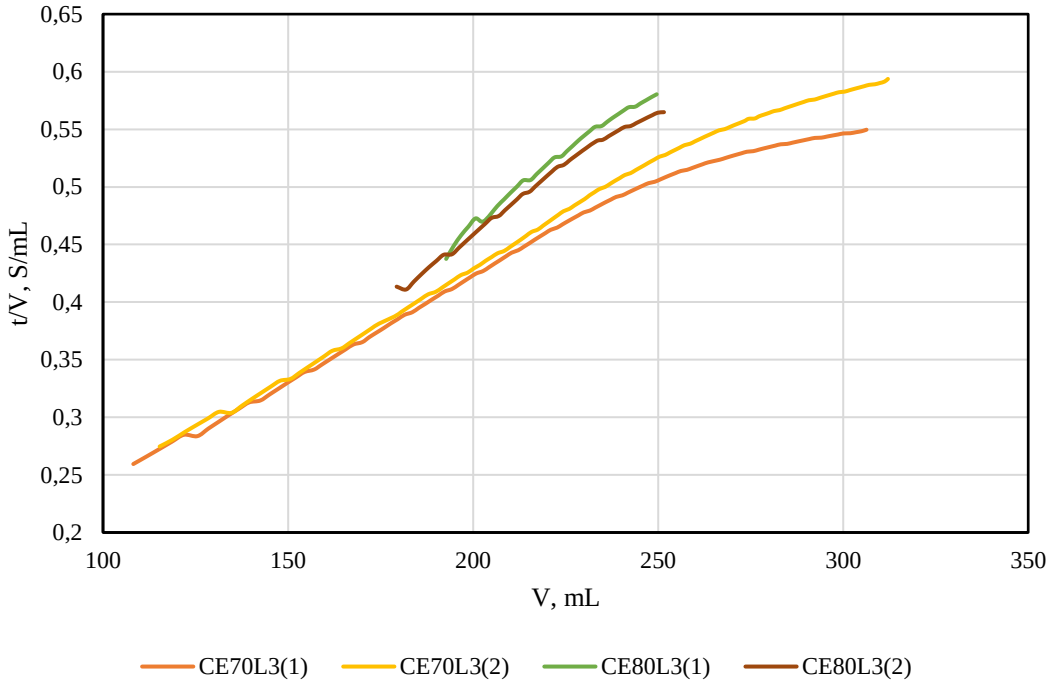

Figure 42 Filterability plots for washed lime mud samples produced from Lime 3 (target CE 70 and 80 %).

Filtration plots for unwashed lime mud samples produced from Lime 4 are shown in Figure 43 and filterability plots in Figure 44, and for washed lime mud samples in Figure 45 and Figure 46 at respective target CE % values.

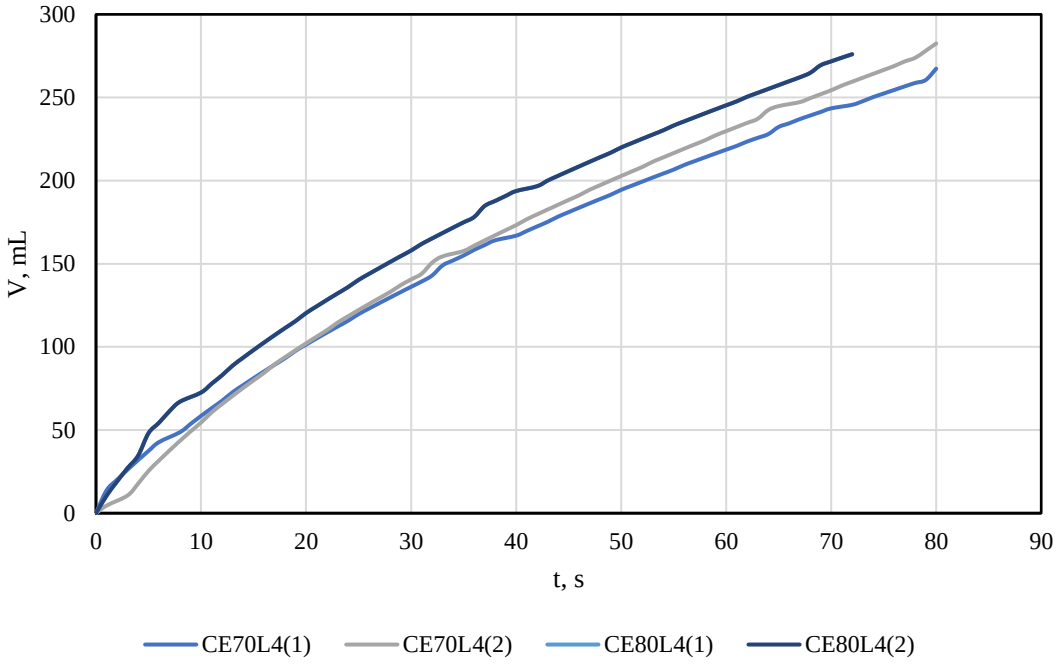

Figure 43 Filtration plots for unwashed lime mud samples produced from Lime 4 (target CE 70 and 80 %).

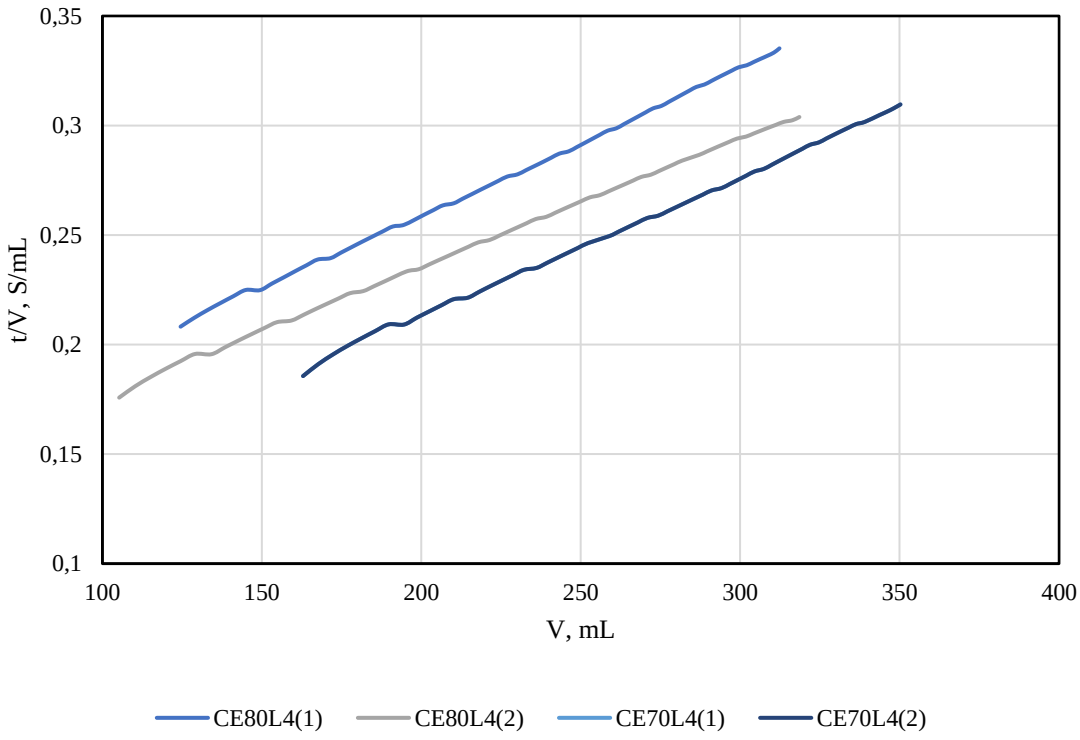

Figure 44 Filterability plots for unwashed lime mud samples produced from Lime 4 (target CE 70 and 80 %).

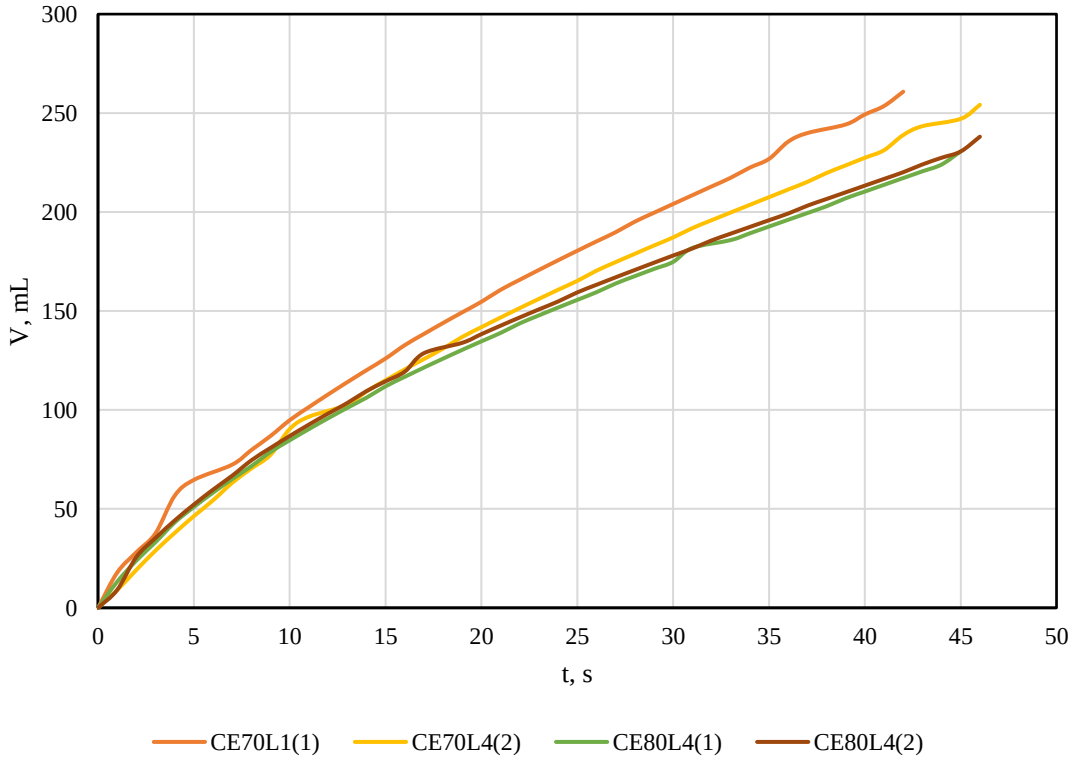

Figure 45 Filtration plots for washed lime mud samples produced from Lime 4 (target CE 70 and 80 %).

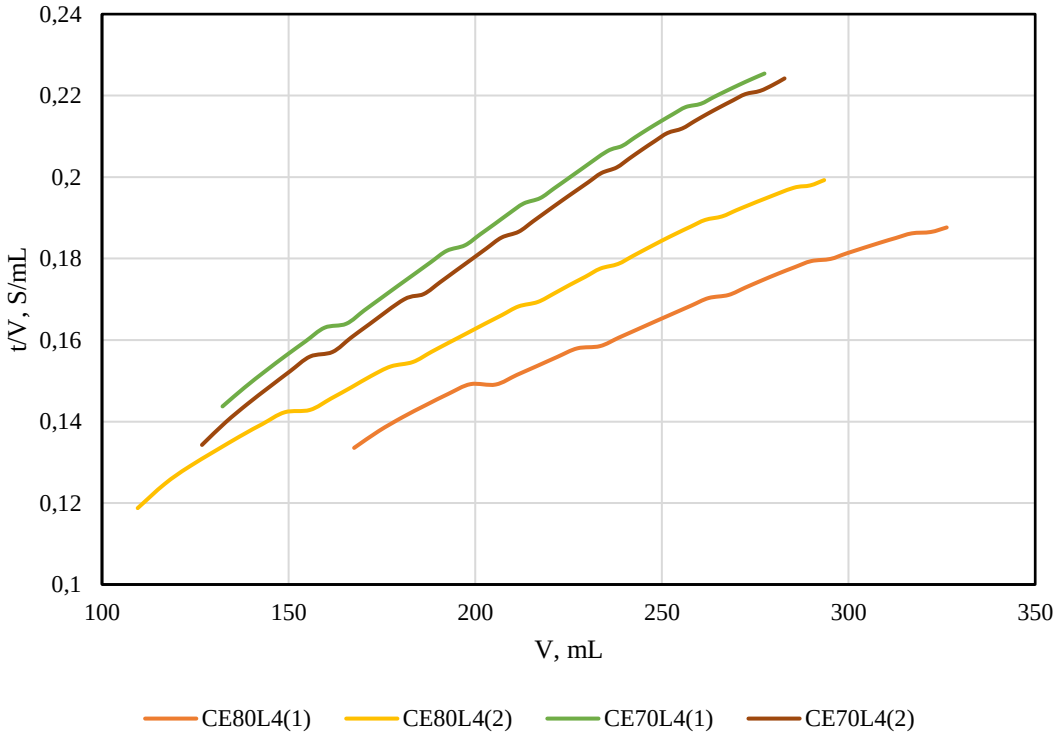

Figure 46 Filterability plots for washed lime mud samples produced from Lime 4 (target CE 70 and 80 %).

Lime mud average porosity and moisture fraction values for both unwashed and washed samples are shown in Table 8.

Table 8 Lime mud porosity and moisture content values across all samples obtained through causticizing experiments in this study. Notation "*CE*" refers to the target CE % of white liquor and "*L*" refers to lime used in causticizing.

Experiment	Unwashed	Washed	Unwashed	Washed
	Porosity, -		Moisture Fraction, -	
CE70L1	-	0.772	-	0.587
CE80L1	-	0.779	-	0.519
CE85L1	0.706	0.775	0.475	0.502
CE70L2B	0.685	0.740	0.382	0.458
CE80L2B	0.688	0.750	0.446	0.462
CE85L2B	0.695	0.760	0.437	0.515
CE70L3	0.686	0.739	0.437	0.438
CE80L3	0.702	0.770	0.405	0.457
CE70L4	0.671	0.772	0.439	0.491
CE80L4	0.746	0.758	0.432	0.522

All zeta potential measurement results are presented in Table 9 for both unwashed and washed samples. Sample solution was prepared by dissolving 0.15 g of lime mud in 500 mL of water. Solution pH was adjusted to 11.5 with white liquor obtained from causticizing.

Table 9 Measured zeta potential values in this study.

Experiment	Zeta Potential (Unwashed), mV	Zeta Potential (Washed), mV
CE70L1(1)	-21.30	-22.63
CE70L1(2)	-24.95	-24.65
CE80L1(1)	-4.14	-3.05
CE80L1(2)	-3.41	-3.99
CE85L1(1)	-1.39	6.19
CE85L1(2)	1.10	2.87
CE70L2B(1)	-11.87	-18.93
CE70L2B(2)	-12.87	-30.57
CE80L2B(1)	-6.26	-5.78
CE80L2B(2)	-12.87	-5.01
CE85L2B(1)	-0.67	7.11
CE85L2B(2)	6.91	10.45
CE70L3(1)	-36.00	-25.77
CE70L3(2)	-32.20	-28.97
CE80L3(1)	-4.99	-7.64
CE80L3(2)	-12.40	-11.55
CE70L4(1)	-29.60	-19.05
CE70L4(2)	-25.97	-19.87
CE80L4(1)	-22.07	-15.67
CE80L4(2)	-24.70	-21.57

Streaming potential records measured by AFG FPA touch! apparatus are shown in Table 10. Sample solution was prepared in distilled water. Solution conductivity was adjusted using white liquor. Note that the zeta potential value here is calculated by the apparatus from measured streaming potential.

Table 10 Measured streaming potential values in this study. Note that the zeta potential value is calculated by the measuring apparatus from measured streaming potential.

Measurement	Conductivity, mS/cm	Streaming Potential, mV	Zeta Potential, mV
CE70L2B(1)	9,32	-0,15	-0,70
CE70L2B(2)	9,51	-0,13	-0,60
CE70L2B(3)	10,43	-0,02	-0,30
CE70L2B(4)	18,05	-0,06	-0,60
CE70L2B(5)	17,20	-0,03	-0,30
CE80L2B(1)	14,66	0,29	2,10
CE80L2B(2)	15,16	0,27	2,00
CE80L2B(3)	15,53	0,22	1,80
CE80L2B(4)	16,84	0,20	1,70
CE80L2B(5)	17,14	0,21	1,80
CE80L2B(6)	16,73	0,24	2,00
CE80L2B(7)	17,22	0,23	2,20
CE85L2B(1)	15,03	0,16	1,20
CE85L2B(2)	15,47	0,16	1,20
CE85L2B(3)	15,66	0,16	1,30
CE85L2B(4)	14,97	0,16	1,20

The determined free lime contents within samples by thermogravimetric analysis (TGA) are shown for unwashed samples in Table 11, and for washed samples in Table 12. $Mg(OH)_2$ content was calculated based on results from ICP analysis.

Table 11 TGA results of determining free lime content within unwashed lime mud samples.

Experiment	Sample mass, mg	$Ca(OH)_2$ weight fraction, -	$m_{Ca(OH)2}$, mg	$Mg(OH)_2$ weight fraction, -	$m_{Mg(OH)2}$, mg	Corrected $Ca(OH)_2$ weight fraction, -
CE70L1	10.240	0.031	0.322	0.015	0.152	0.017
CE80L1	11.300	0.048	0.540	0.015	0.167	0.033
CE85L1	10.780	0.077	0.825	0.015	0.160	0.062
CE70L2B	10.800	0.039	0.421	0.009	0.095	0.030
CE80L2B	10.430	0.057	0.595	0.009	0.092	0.048
CE85L2B	13.180	0.067	0.876	0.009	0.116	0.058
CE70L3	10.770	0.029	0.313	0.010	0.108	0.019
CE80L3	10.580	0.044	0.461	0.010	0.107	0.034
CE70L4	10.730	0.033	0.358	0.008	0.081	0.026
CE80L4	10.540	0.036	0.375	0.008	0.080	0.028

Table 12 TGA results of determining free lime content within washed lime mud samples.

Experiment	Sample mass, mg	$Ca(OH)_2$ weight fraction,-	$m_{Ca(OH)2}$, mg	$Mg(OH)_2$ weight fraction, -	$m_{Mg(OH)2}$, mg	Corrected $Ca(OH)_2$ weight fraction,-
CE70L1	10.130	0.028	0.285	0.015	0.150	0.013
CE80L1	10.080	0.039	0.396	0.015	0.149	0.024
CE85L1	11.000	0.064	0.708	0.015	0.163	0.050
CE70L2B	11.970	0.029	0.347	0.009	0.106	0.020
CE80L2B	11.680	0.042	0.488	0.009	0.103	0.033
CE85L2B	10.270	0.055	0.566	0.009	0.091	0.046
CE70L3	10.660	0.013	0.142	0.010	0.107	0.003
CE80L3	12.640	0.029	0.368	0.010	0.127	0.019
CE70L4	10.460	0.023	0.238	0.008	0.079	0.015
CE80L4	10.790	0.022	0.236	0.008	0.082	0.014